

AD-A245 474



✓ (2)

# A TRIDENT SCHOLAR PROJECT REPORT

NO. 186

---

OPTICAL STRAIN MONITORING IN  
COMPOSITE MATERIALS

---

DTIC  
ELECTE  
FEB 06 1992  
S D D



UNITED STATES NAVAL ACADEMY  
ANNAPOLIS, MARYLAND

This document has been approved for public  
release and sale; its distribution is unlimited.

92-02851



92 2 04 013

U.S.N.A. - Trident Scholar project report; no. 186 (1991)

**OPTICAL STRAIN MONITORING IN COMPOSITE MATERIALS**

**A Trident Scholar Project Report**

by

Midshipman First Class Daniel B. Robinson  
Class of 1991  
United States Naval Academy  
Annapolis, Maryland

*Olaf M. Rask*

Associate Prof. O. N. Rask  
Advisor - Systems Eng. Dept.

Accepted for Trident Scholar Committee

*Francis D. Cornell*

Chair

*13 May 1991*

Date

Accession For	
NTIS CRA&I	<input checked="checked" type="checkbox"/>
DTIC TAB	<input type="checkbox"/>
Unannounced	<input type="checkbox"/>
Justification	
By	
Distribution/	
Availability Codes	
Dist	Avail and/or Special
A-1	



USNA-1531-2

# REPORT DOCUMENTATION PAGE

Form Approved  
OMB No. 0704-0188

Public reporting burden for this collection of information is estimated to average 1 hour per response, including the time for reviewing instructions, searching existing data sources, gathering and maintaining the data needed, and completing and reviewing the collection of information. Send comments regarding this burden estimate or any other aspect of this collection of information, including suggestions for reducing this burden, to Washington Headquarters Services, Directorate for Information Operations and Reports, 1215 Jefferson Davis Highway, Suite 1204, Arlington, VA 22202-4302, and to the Office of Management and Budget, Paperwork Reduction Project (0704-0188), Washington, DC 20503.

1. AGENCY USE ONLY (Leave blank)		2. REPORT DATE 13 May 1991		3. REPORT TYPE AND DATES COVERED Final 1990/91	
4. TITLE AND SUBTITLE OPTICAL STRAIN MONITORING IN COMPOSITE MATERIALS				5. FUNDING NUMBERS	
6. AUTHOR(S) Daniel B. Robinson					
7. PERFORMING ORGANIZATION NAME(S) AND ADDRESS(ES) U.S. Naval Academy, Annapolis, MD				8. PERFORMING ORGANIZATION REPORT NUMBER U.S.N.A. - TSPR; 186 (1991)	
9. SPONSORING/MONITORING AGENCY NAME(S) AND ADDRESS(ES)				10. SPONSORING/MONITORING AGENCY REPORT NUMBER	
11. SUPPLEMENTARY NOTES Accepted by the U.S. Trident Scholar Committee.					
12a. DISTRIBUTION/AVAILABILITY STATEMENT This document has been approved for public release; its distribution is UNLIMITED.				12b. DISTRIBUTION CODE	
13. ABSTRACT (Maximum 200 words) Composite materials are substances made up of at least two components. Typically, one phase is fibrous and the second phase is a resin. The fibers provide the strength while the resin supports and protects the fibers. Optical fibers embedded within a composite structure during its layup offer a means of monitoring the structure. This project studied two different types of monitoring. Both utilized the Mach-Zehnder interferometer configuration. The first provided a signal that was used to obtain a detailed calibration for the optical strain gauge as the composite beam was deflected in three point bending. The second provided a signal in the audio spectrum that was used to monitor a composite specimen under various driving forces. This signal was evaluated subjectively and also quantitatively through the use of a computer.					
14. SUBJECT TERMS Composite materials Optical fibers Interferometry				15. NUMBER OF PAGES 62	
				16. PRICE CODE	
17. SECURITY CLASSIFICATION OF REPORT UNCLASSIFIED	18. SECURITY CLASSIFICATION OF THIS PAGE UNCLASSIFIED	19. SECURITY CLASSIFICATION OF ABSTRACT UNCLASSIFIED	20. LIMITATION OF ABSTRACT		

## ABSTRACT

Composite materials are substances made up of at least two components. Typically one phase is fibrous and the second phase is a resin. The fibers provide the strength while the resin supports and protects the fibers. Optical fibers embedded within a composite structure during its lay-up offer a means of monitoring the structure.

This project studied two different types of monitoring. Both utilized the Mach-Zehnder interferometer configuration. The first provided a signal that was used to obtain a detailed calibration for the optical strain gauge as the composite beam was deflected in three point bending. The second provided a signal in the audio spectrum that was used to monitor a composite specimen under various driving forces. This signal was evaluated subjectively and also quantitatively through the use of a computer.

Although the first experiment showed that the optical strain gauge studied is about as sensitive to mechanical strain as conventional foil strain gauges, the output does not represent a one to one correspondence to actual strain. It can be shown that the output is actually the cosine of the integral of strain over the length of the fiber within

the specimen. A more complicated optical strain gauge is necessary to solve for the actual strain. This system shows much more promise as a subjective indicator of damage or flaws in a structure than it does as a simple strain gauge.

## TABLE OF CONTENTS

I. Introduction.....	4
II. Specimen Preparation.....	8
III. Experimental Setup.....	12
A. First Experiment.....	12
B. Second Experiment.....	14
IV. Theory of the Strained Optical Fibers.....	18
V. Optical Strain Measurements in Composite Structures.....	19
VI. Audio Spectrum Analysis of Output.....	21
VII. Results.....	23
A. First Experiment.....	23
B. Second Experiment.....	26
C. Limitations.....	40
VIII. Conclusion .....	43
IX. Applications.....	44
X. Future Work.....	44
XI. Bibliography.....	46
XII. Appendices.....	49

## INTRODUCTION

Composite materials are substances made up of at least two distinct components which together have properties superior to those of the individual components. Typically one phase is fibrous and the second phase is a resin. The fibers provide the strength while the resin supports and protects the fibers. Combinations include carbon, Kevlar, and glass fibers held together in a variety of resins. Resins include epoxy, vinyl ester and poly ester.

Due to their light weight, ease of molding into different shapes, and resistance to corrosion, these materials are being used in many areas, most notably in air and spacecraft design. Presently composites account for 10% of the weight of one tactical aircraft, the F/A-18 Hornet. In addition, most helicopter rotor blades are made of composites.

As military aircraft become more advanced, the structure of the aircraft can withstand more stress than the pilots who fly them. Thus research and development is turning away from increasing maneuverability, and more toward increasing range and payload. To achieve these, industry is depending on composite materials because they offer the same strength as traditional metals, yet can be up to nineteen times lighter.

Although composites are stiff, strong, and lightweight, they can fail without warning, unlike metals which often show outward signs of fatigue, such as cracking, before they fail. Since the use of composites is relatively new, there is little experience in estimating the life span of a composite structure. A means of sensing strain and structural integrity throughout the material would provide valuable information.

In a Trident project completed in 1987, Midshipman David Robinson proposed the use of electrical resistance of the graphite in a graphite-epoxy composite as a means of monitoring the structure.<sup>1</sup> He showed that the resistance varied uniformly with mechanical strain; however, the electrical contacts used were very fragile and could withstand very little strain. Due to this characteristic they were not practical for use in an actual structure. Another system for monitoring structural condition employs optical fibers which are embedded within the structure. This system will work with any fibrous material, independent of its electrical conductivity. It works because the resin transfers the mechanical strain of the structure to the optical fibers.

Optical fiber systems for measuring mechanical strain

---

<sup>1</sup>Robinson, David A., "Failure Modes in Composite Materials," USNA Trident Scholar Project Report, No. 148(1987).

were proposed as early as 1978.<sup>2</sup> The configuration most frequently discussed is shown in Fig. 1. It is the fiber optic equivalent of the Mach-Zehnder interferometer. In it, coherent light from a Helium-Neon laser is focused into an optical fiber which is then divided into two fibers traversing different paths within a structure. When the fibers exit the structure, they are recombined into a single fiber, the light from which is focused onto a solid state photodetector. As the structure undergoes mechanical strain, the lengths of the two fibers within the structure will change. If any difference is created in the strained lengths of the two embedded fibers, the phases of the light waves out of them will change and so create fluctuations in the photodetector signal.

Recent developments in optical strain measurements have used the Michelson interferometer configuration.<sup>3</sup> This technique was not considered in this work. It seems to offer a totally different set of practical considerations.

These are just two examples of the class of structural monitoring systems now known generally as smart skins. With frequent emphasis on applications in air and spacecraft design, the basic notion is that if sensors can be

---

<sup>2</sup>Butler, C. D. and G. B. Hocker, "Fiber Optics Strain Gauge," Applied Optics, Vol 17(1978), pp. 2667-2669.

<sup>3</sup>Valis, T., et al., "Localized Fiber Optics Strain Sensors Embedded in Composite Materials," Fiber Optic Smart Structures and Skins II, SPIE, Vol 1170(1990), pp 495-504.

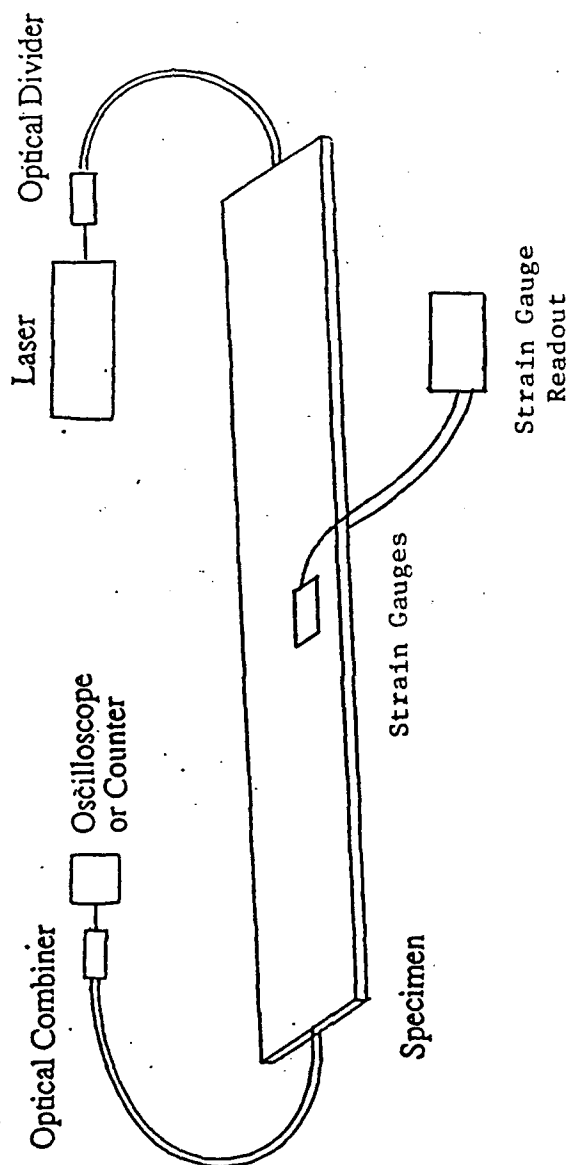


FIG. 1  
Mach-Zehnder Interferometer

permanently embedded within critical regions of the structure, the strain and mechanical integrity can be monitored in real time. The system is particularly attractive for composite structures because the optical fibers are sufficiently small that they can be included within the structure as it is formed with negligible effect on its mechanical or aerodynamic properties.<sup>4</sup>

In this work two different aspects of the optical strain gauge were studied. In the first experiment a detailed calibration for the optical strain gauge was obtained. In the second experiment, the optical strain gauge was studied as a qualitative tool in detecting changes in a mechanical structure under normal operational forces.

### **SPECIMEN PREPARATION**

The basic materials used to construct the composite specimens included 7.2 oz./sq. yd. E Glass unidirectional fiberglass cloth, York SM600 single mode optical fibers and a two part System West epoxy matrix compound. The configuration for the first experiment is shown in Fig. 2. In it a single optical fiber was placed in a thin coat of resin over which four layers of fiberglass cloth saturated

---

<sup>4</sup>Tay, A., and D. Wilson, "Strain Analysis of Optical Fibers Embedded in Composite Materials Using Finite Element Modeling," Fiber Optic Smart Structures and Skins II, SPIE, Vol 1170(1990), pp. 521-533.

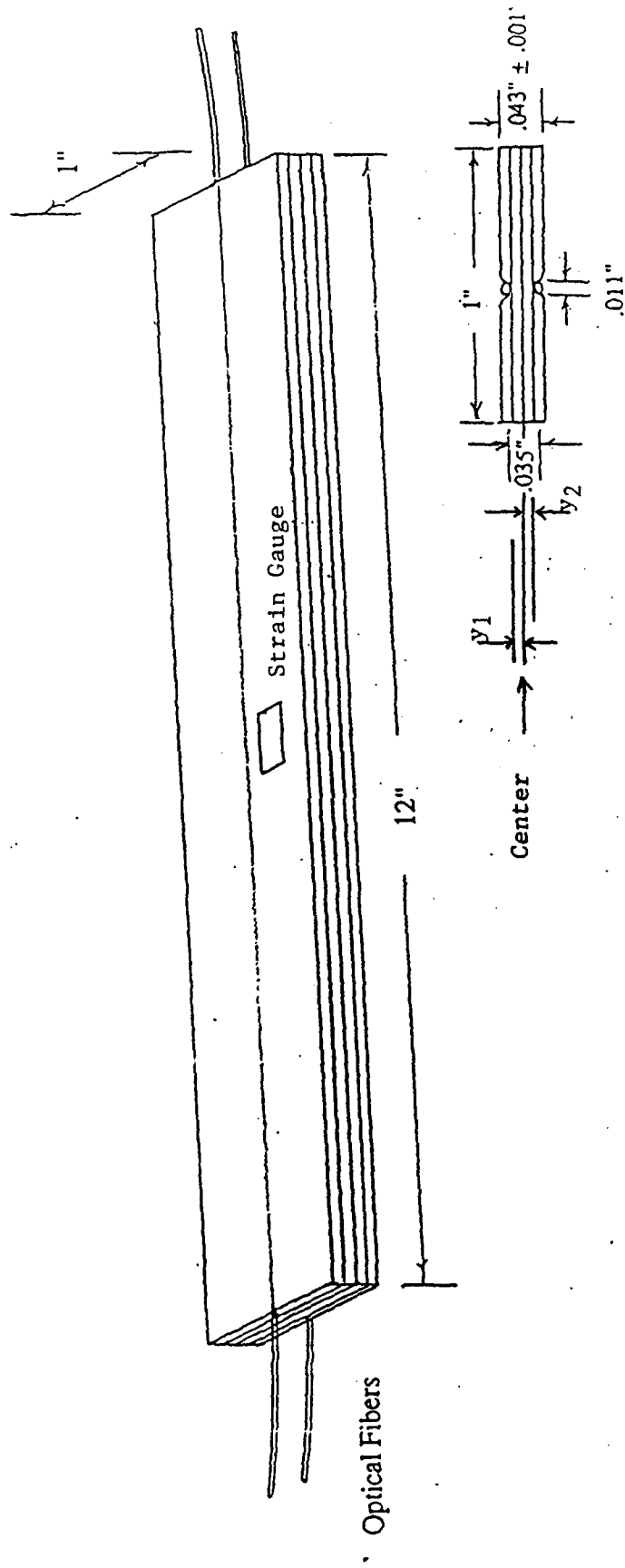


FIG. 2  
Geometry of Specimen used  
in First Experiment

in resin were placed. The second optical fiber was added on top, and finally a layer of peel ply was put down to soak up excess resin. The resulting specimen was allowed to cure for over twenty four hours. This was done on a Formica surface from which the specimen could be easily removed after hardening. The specimen was then trimmed to appropriate dimensions and was ready for experimentation.

The configuration for the second experiment is shown in Fig. 3. The optical fibers were separated by eight layers of fiberglass cloth in the center of the specimen. Four additional layers were placed outside the fibers.

The geometry of this specimen was determined by two factors. First, the fibers had to both enter and exit the specimen at one end to allow the other end to be free to vibrate. The loops of optical fiber within the specimen had to have a sufficiently large radius of curvature to prevent light leakage.<sup>5</sup> This required a large "turn around" area at the free end of the specimen. Second, the electrical signal generated by the optical fiber was required to be in the audible frequency range. This constraint related the resonant frequency of the composite specimen to the fiber separation within the specimen. The total thickness of the specimen determined the resonant frequency, and the resonant frequency along with the fiber separation determined the

---

<sup>5</sup>Jones, W. B., Introduction to Optical Fiber Communication Systems, Holt, Rinehart and Winston, Inc., New York, 1988.

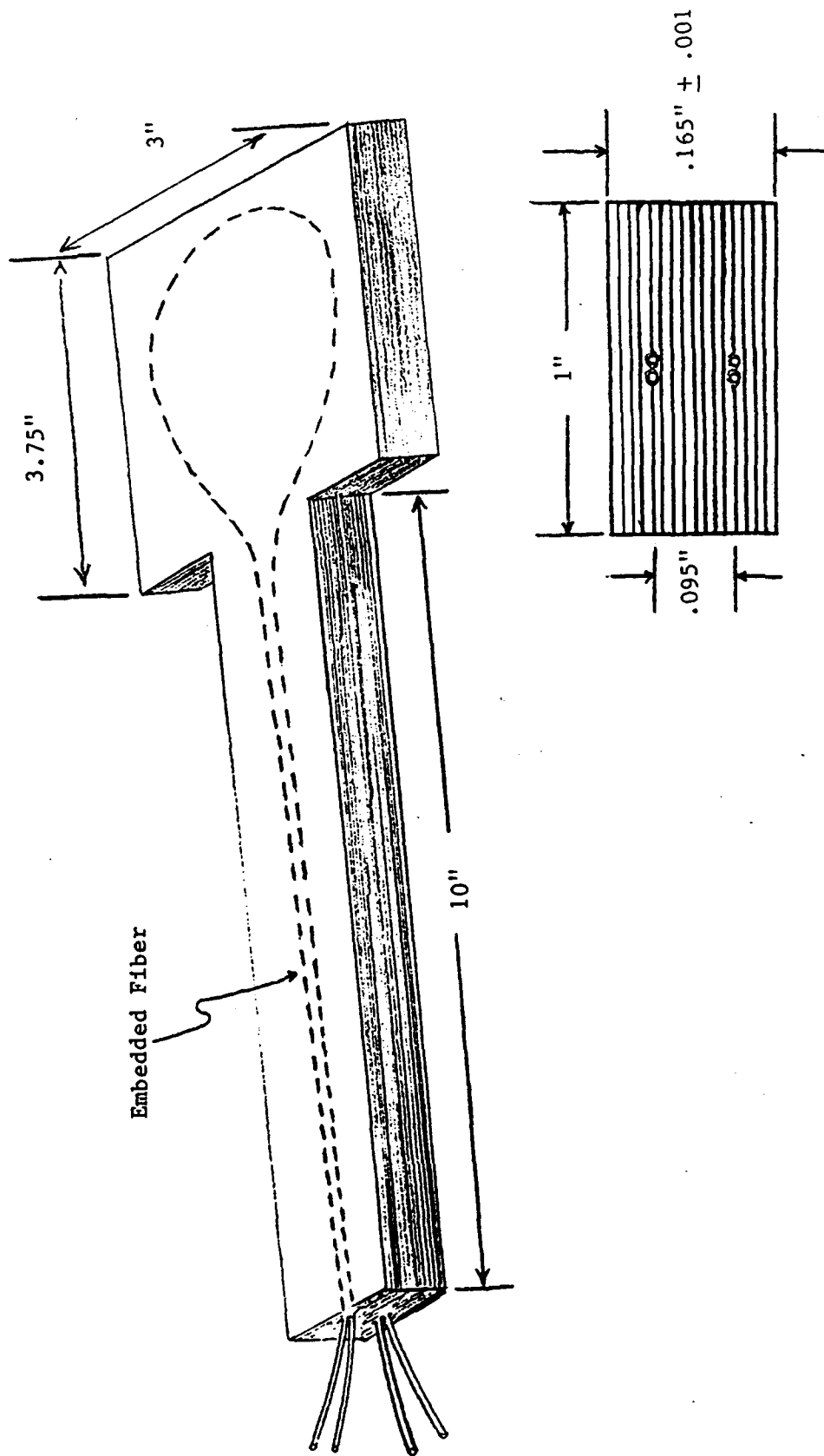


FIG. 3  
Geometry of Specimen used  
in Second Experiment

audio frequency of the output signal.

## **EXPERIMENTAL SETUP**

### **1. First Experiment**

The first of the two experiments is illustrated in Fig. 4. It was intended to calibrate the York SM600 communication fiber which was used in the experiment. In it a unidirectional fiberglass/epoxy composite beam with the two optical fibers, one on the top and one on the bottom, was placed in three point bending. Conventional foil strain gauges were also placed on the top and the bottom of the beam. The beam was then deflected in one direction with a micromanipulator, and after every 100 current peaks the deflection,  $D$ , was measured and the foil strain gauge readings were recorded. Long before the specimen reached its linear limit, the deflection was halted and the measurements repeated as the deflection was relaxed. To check on any asymmetry within the hand lay-up specimen, it was deflected in the other direction by turning it over in the three point holder. No significant asymmetries were found.

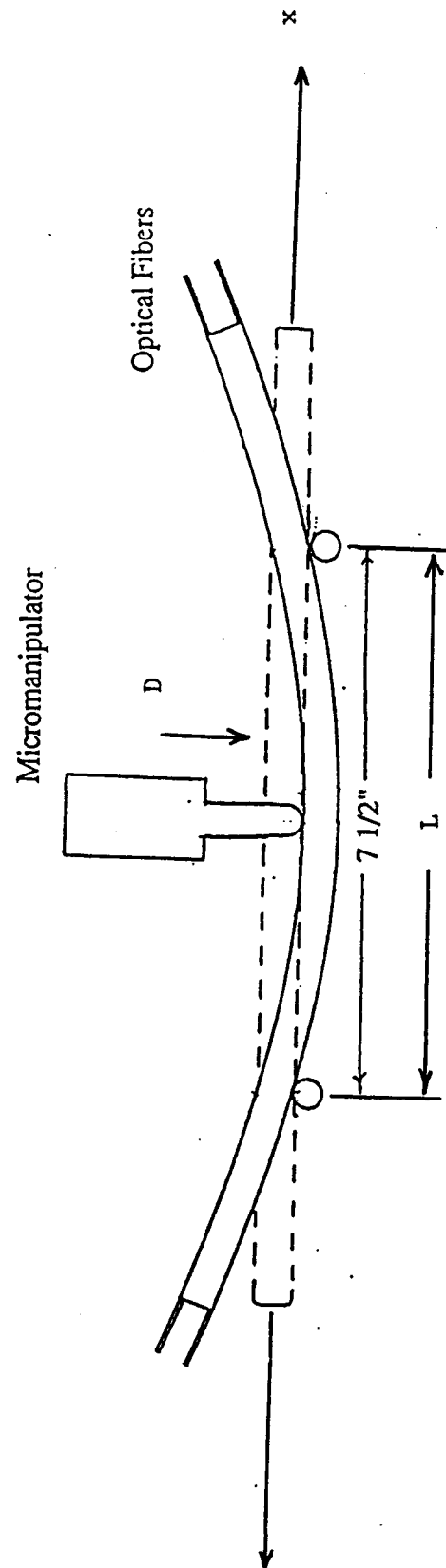


FIG. 4  
Configuration of First Experiment

## 2. Second Experiment

The second experiment is illustrated in Fig. 5. It was intended to test the use of the system as a qualitative means of detecting various changes in a structure. In it a unidirectional fiberglass/epoxy composite beam, sketched in Fig. 3, was mounted vertically in a wind tunnel and subject to cantilever deflection. The specimen differs slightly from the one used in the first experiment in that the fibers enter and exit at the base of the specimen. The fibers can be positioned within the specimen so that, for typical operating stresses, the output signal lies in the audio frequency range. The actual output depends on the time dependent strain experienced by the specimen. The idea behind the experiment is that the output signal as encoded by the optical strain gauge is in a format that is particularly well suited to subjective audio analysis by a human observer.

A special mass, sketched in Fig. 6, was fixed to the free end of the beam resulting in a lightly damped resonant mechanical structure. Also, an additional aerodynamic surface could be fixed to the free end of the beam. No attempt was made to analyze the exact motion of any of these mechanical variations. The needs of the experiment were met by any structure which could easily be changed and which contained an optical strain gauge with its output in the

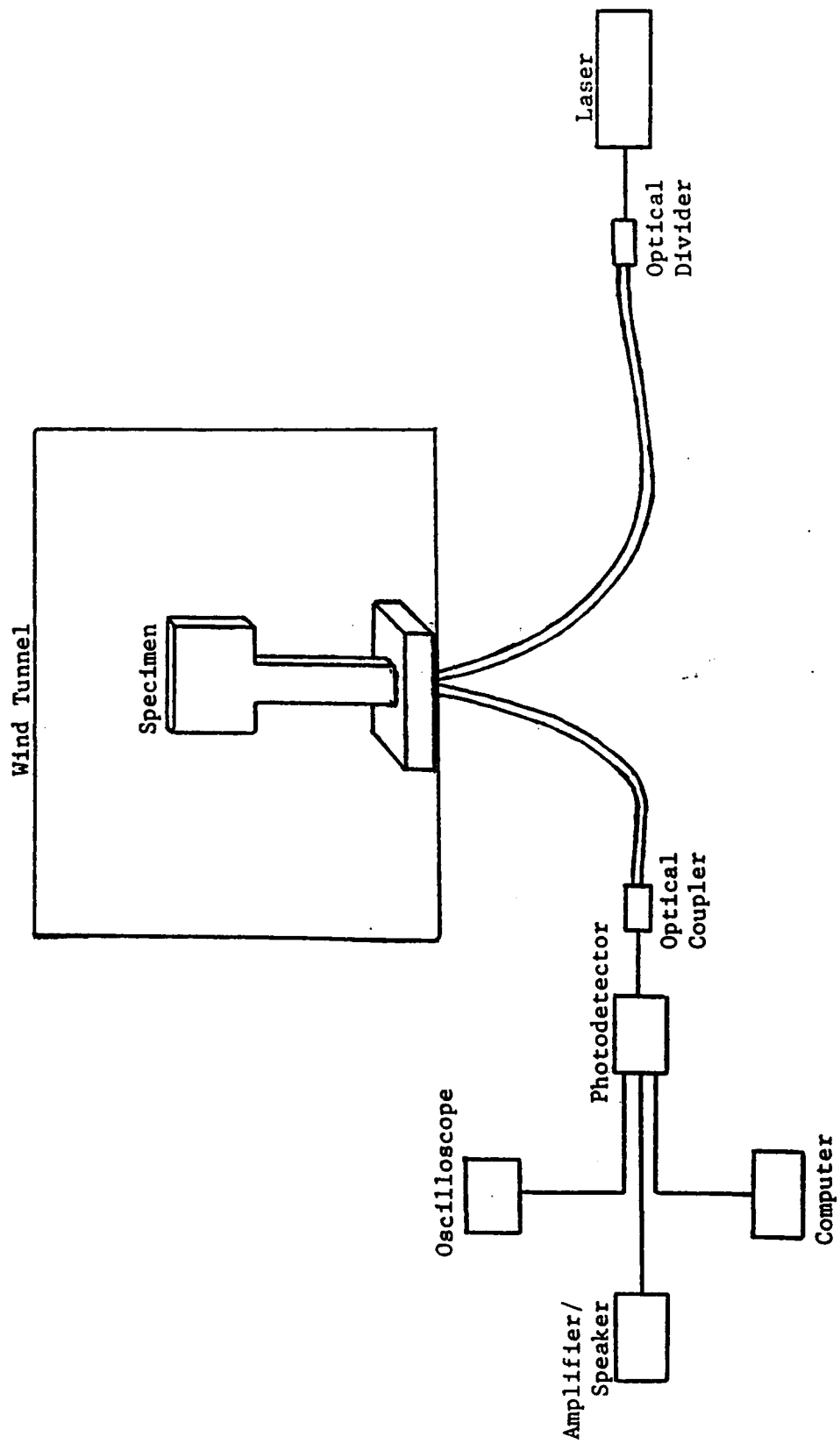


FIG. 5  
Configuration of Second Experiment

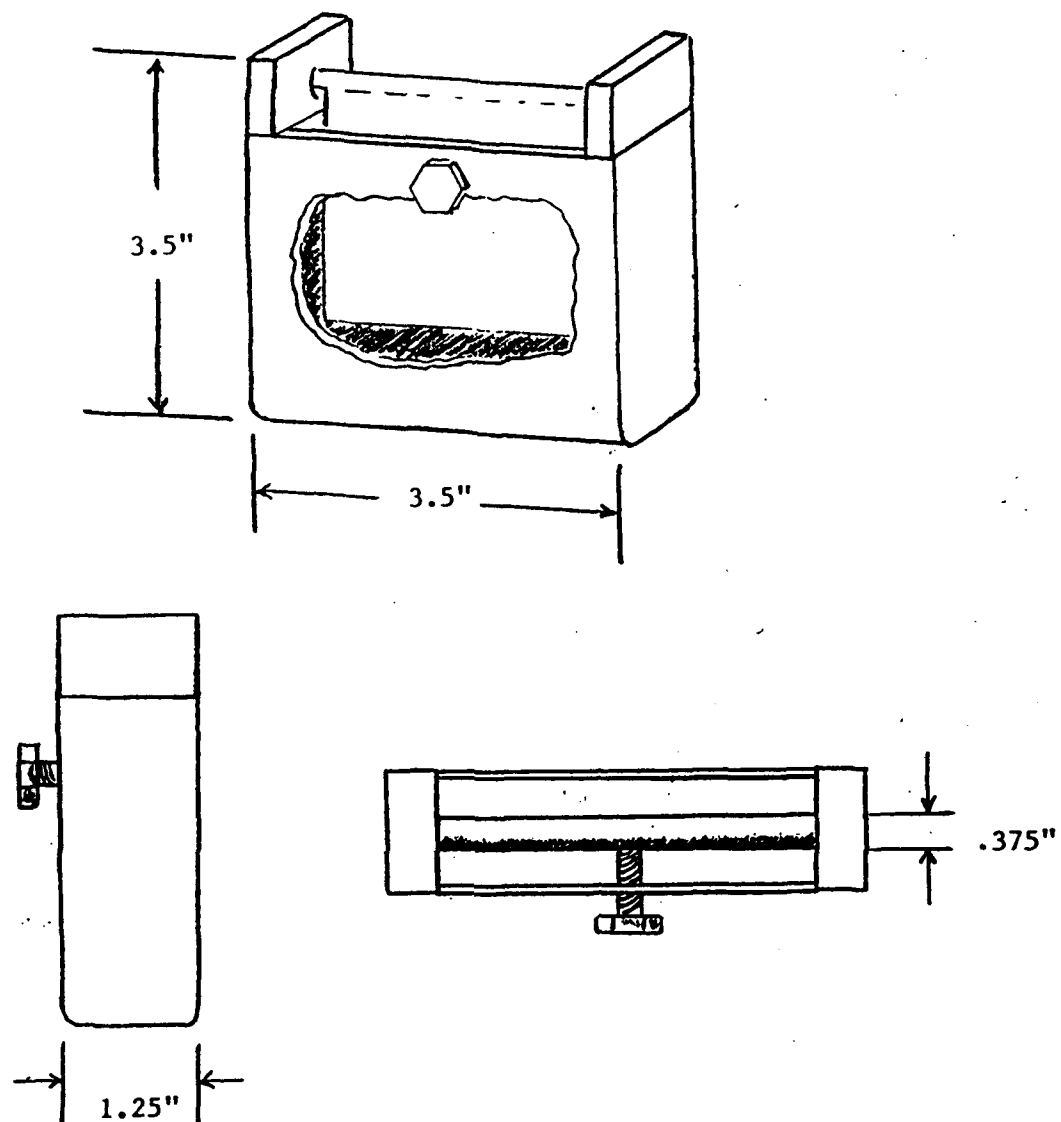


FIG. 6  
Diagram of Mass

audio frequency range. The mass consisted of a pendulum mounted in a box with adjustable hard limits on the amplitude of its swing. With these limits set to zero, it became a simple point mass in a second order system. This particular mechanical variation modeled an undamaged system. With the limits open, so that the pendulum could swing between the hard limits, the overall system became a nonlinear fourth order system. The additional aerodynamic surface was added to obtain another mechanical variant, probably best modeled as a sixth order nonlinear system. These later variations modeled different damaged systems.

In all cases, the free end of the beam was displaced by hand to an initial amplitude,  $A$ , and then released. The resulting signals from the photodetector were recorded on a commercial tape recorder and also put into an amplifier/speaker system for subjective evaluation. They modeled the impulse responses of the intact and the various damaged mechanical systems.

In the final portion of the second experiment, the beam was driven by turbulent forces of the wind while the wind tunnel was running. The signals for the simulated intact and damaged structures were recorded for subjective evaluation. Finally the noise created in the optical system due to the wind tunnel machinery running but generating no wind was recorded.

The signals on the tape were later sampled and stored

in a file in a PC where its power spectral density was calculated using MATLAB software as described in Appendix C. Typical time and frequency plots are shown in Figs. 8 to 19.

### THEORY OF THE STRAINED OPTICAL FIBERS

When coherent, monochromatic light from the two fibers in the interferometer is summed at the photodetector, the photodetector current can be shown to be given by the expression in Eq. 1. Here  $\phi_1$  and  $\phi_2$  are the phases of the light out of the two fibers, and  $E$  is the light amplitude, assumed equal for the two fibers.

$$i = E^2 (1 + \cos(\phi_1 - \phi_2)) \quad (1)$$

The phase of the light out of an unstrained fiber of length,  $dx$ , is given in Eq. 2.

$$\phi = \left( \frac{2\pi n}{\lambda_0} \right) (dx) \quad (2)$$

Here  $n$  is the index of refraction of the material and  $\lambda_0$  is the free space wavelength. In this experiment,  $n = 1.5$  and  $\lambda_0 = .63$  microns. When the optical fiber is strained, there is a change in phase,  $\Delta\phi$ , given in Eq. 3.

$$\Delta\phi = \left(\frac{2\pi}{\lambda_0}\right) (n \cdot \Delta dx + \Delta n \cdot dx) \quad (3)$$

The term,  $n \cdot \Delta dx$ , represents merely the phase change due to the increase in length of the segment of fiber,  $dx$ .

The change in the index of refraction,  $\Delta n$ , is shown in Ref. 1 to be proportional to the mechanical strain,  $\epsilon$ .

$$\Delta n = -C \cdot \epsilon = -C \cdot \frac{\Delta(dx)}{dx} \quad (4)$$

Here  $C$  is a positive number that contains numerous physical constants of the material which, for commercially available communication fibers, are difficult find. The actual goal of this portion of the experiment is the empirical measurement of this constant. Realizing that  $\Delta dx = \epsilon dx$  and uniting Eq. 3 and Eq. 4, we obtain Eq. 5.

$$\Delta\phi = \left(\frac{2\pi}{\lambda_0}\right) (n - C) (\epsilon dx) \quad (5)$$

The constant,  $C$ , is best understood as the decrease per unit strain of the index of refraction due to reduced material density of the fiber corresponding to its elongation.

#### OPTICAL STRAIN MEASUREMENTS IN COMPOSITE STRUCTURES

Elementary beam theory, as outlined in Appendix A, can

be used to obtain Eqs. 6, 7, and 8. The shape of the beam in terms of its deflection,  $D$ , is given in Eq. 6. Fig. 4 shows the geometry.

$$y = \frac{24 * D}{L^3} * \left( \frac{L}{4} * x^2 - \frac{1}{6} * x^3 \right) \quad (6)$$

At any point along the beam, its curvature,  $K$ , is given by the expression in Eq. 7.

$$K = \frac{d^2 y}{dx^2} = \left( \frac{24D}{L^3} \right) * \left( \frac{L}{2} - x \right) \quad (7)$$

The longitudinal strain within the beam as a function of distance,  $y$ , from the center is given in Eq. 8, as derived in Appendix B.

$$\epsilon = -y * K \quad (8)$$

When the fiber distance,  $y_1$ , shown in Fig. 2 is substituted into Eq. 8, Eq. 8 can be substituted into Eq. 5 to calculate the phase change,  $\Delta\phi_1$ , for each  $dx$  along the upper surface of the beam due to a deflection,  $D$ . This is given in Eq. 9.

$$\phi_1 = -\frac{12\pi D}{\lambda_0 L} (n-C) (y_1) \quad (9)$$

Integrating over the beam length will give the total phase change,  $\phi_1$ , for the top fiber. This is given in Eq. 10.

$$\phi_1 = \left( \frac{2\pi}{\lambda_0} \right) (n-C) (-y_1) \left( \frac{24D}{L^3} \right) \int_{-L/2}^{L/2} \left( \frac{L}{2} - x \right) dx = -\frac{12\pi D}{\lambda_0 L} (n-C) (y_1) \quad (10)$$

The calculation is repeated for the bottom fiber to obtain  $\phi_2$ . The difference,  $\phi_1 - \phi_2$ , is the relative optical phase change and is shown in Eq. 11.

$$\phi_1 - \phi_2 = -\frac{12\pi D}{\lambda_0 L} (n-C) (y_1 - y_2) \quad (11)$$

Dividing by  $2\pi$ , the expression in Eq. 12 gives the number of peaks as a function of D. The plot is in Fig. 7.

$$P = \left( \frac{6D}{\lambda_0 L} \right) (n-C) (|y_1| + |y_2|) \quad (12)$$

#### AUDIO SPECTRUM ANALYSIS OF OUTPUT

In the second experiment the Mach-Zehnder optical interferometer was used in a more qualitative manner. For

$$I = E^2 \left( 1 + \cos \left( \frac{12\pi D(t)}{\lambda_0 L} (n-C) (|y_1| + |y_2|) \right) \right) \quad (13)$$

the specimen in Fig. 2, the gauge output,  $i$ , given in Eq. 13, relates the gauge current to the displacement,  $D(t)$ .

The optical strain gauge encodes the displacement,  $D(t)$ , into an audio signal whose frequency is the first time derivative of  $D(t)$ . While there were few apparent differences in the actual motions of the different mechanical systems, the optical strain gauge signals could easily be distinguished by ear. That is, when the optical strain gauge encoded mechanical displacements into an audio signal, small differences in motion became apparent.

If we approximate  $D(t)$  with a cosine function as in Eq. 14, one additional step can be taken.

$$i = E^2 (1 + \cos((Az) \cos(\omega t))) \quad (14)$$

The constant,  $z$ , depends on the particular specimen and  $A$  is the amplitude of its mechanical oscillation. Using the familiar identity for a cosine of a cosine, the expression in Eq. 15 results.<sup>6</sup>

$$i = E^2 (1 + (J_0(Az) + \sum_{k=1}^{\infty} (-1)^k J_{2k}(Az) \cos(2k\omega t))) \quad (15)$$

---

<sup>6</sup>Handbook of Mathematical Functions, National Bureau of Standards, Applied Mathematics Series 55, (June 1964), p.355.

As in an FM modulation scheme, the greater A, the higher the frequency content of the signal.

## RESULTS

### 1. First Experiment

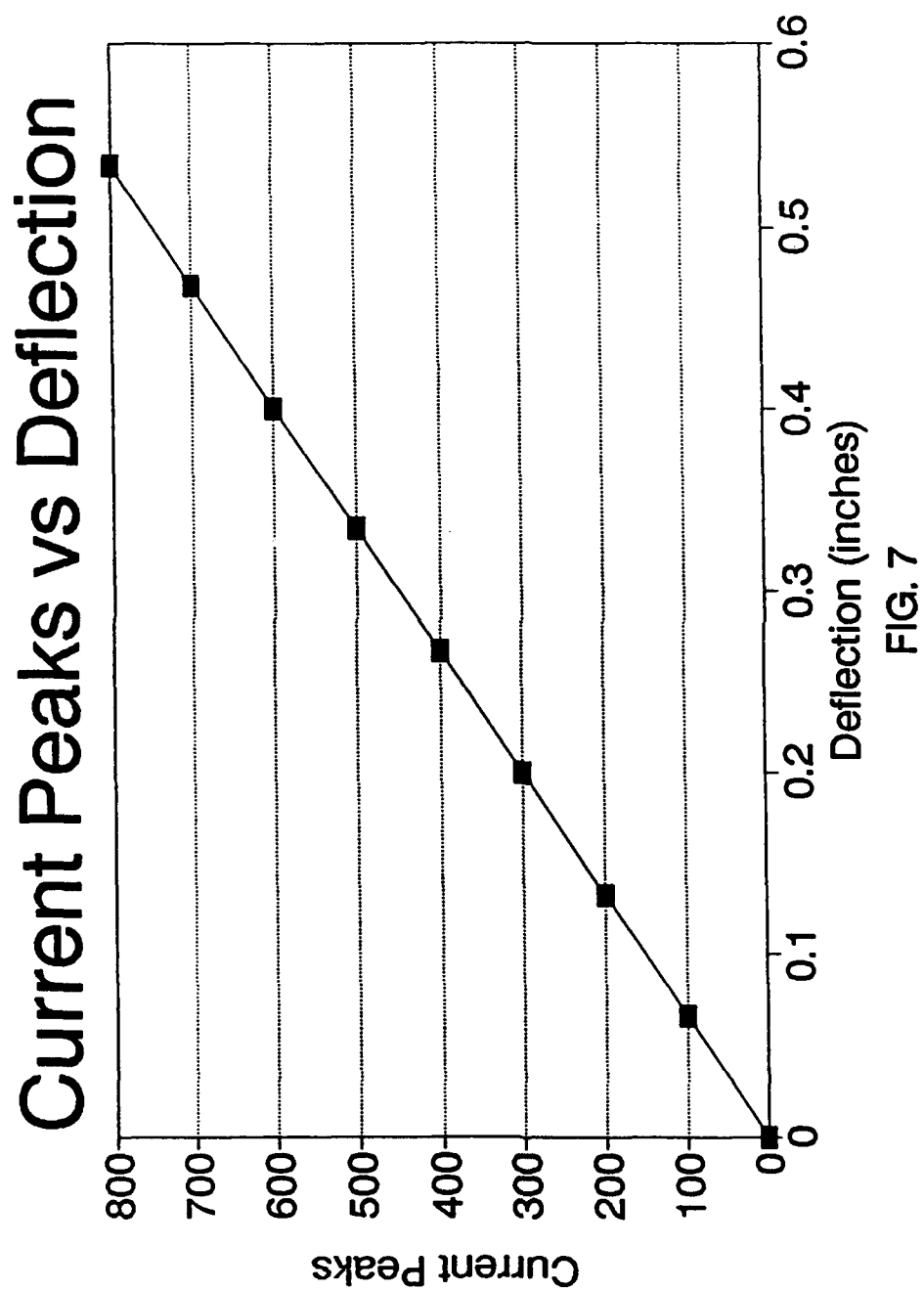
Table 1 shows typical data obtained in the three point deflection of the composite beam shown in Fig. 2. Fig. 7 shows a plot of this data. The slope of the linear relation in Eq. 12 contains the constant, C, and, for a best fit to the data,  $C = 0.165$ . The intrinsic sensitivity of the gauge can be calculated from Eq. 5. The change in phase per unit length per unit strain is measured to be  $0.336 \times 10^6$  radians/inch. This figure agrees to within a 6% of that obtained in the work in Ref. 2 and compares with normal foil strain gauges. For example, a 0.5 inch length of fiber will have a strain resolution  $18.7 \times 10^{-6}$ . This is typical of ordinary foil strain gauges.

The readings of the conventional foil strain gauges were used only to confirm the values of strain calculated from the deflection, D. Concern is frequently voiced over the use of conventional foil strain gages on composite materials. No difficulties were found in this experiment and foil strain gauge readings might be useful in calibrating an optical gauge system with more complex geometry.

TYPICAL DATA

Deflection in Inches	Strain in 10 <sup>-6</sup>	Fringe Count
.000	0	0
.066	292	100
.133	586	200
.200	877	300
.267	1170	400
.334	1461	500
.400	1750	600
.468	2040	700
.534	2324	800

TABLE 1



## 2. Second Experiment

Typical time domain and frequency domain plots obtained in the second experiment are shown in Fig. 8 to Fig. 19. Table 2 summarizes the experimental conditions corresponding to these Figures. It was not difficult to detect differences in the behavior of the specimen in the various configurations simply by listening to the audio signals. By contrast, finding differences in the frequency domain plots proved difficult. Within the limits of available resources, differences could not be detected. In the time domain, however, the presence of nonlinearities were often obvious for sufficiently large amplitudes of the specimen. It should be noted that as the amplitude decreased, a threshold was reached when the pendulum stopped swinging within the box, and the specimen resumed behavior characteristic of the undamaged condition. This transition was obvious by observing the time domain plots as well as by listening to the signal.

## SUMMARY OF RESULTS

FIGURE	DOMAIN	PENDULUM	WIND TUNNEL	ADDITIONAL AERODYNAMIC STRUCTURE
8	Time	Tight	Off	None
9	Frequency	Tight	Off	None
10	Time	Loose	Off	None
11	Frequency	Loose	Off	None
12	Time	Tight	Off	Added
13	Frequency	Tight	Off	Added
14	Time	Loose	Off	Added
15	Frequency	Loose	Off	Added
16	Time	Tight	On	None
17	Frequency	Tight	On	None
18	Time	Loose	On	None
19	Frequency	Loose	On	None

TABLE 2

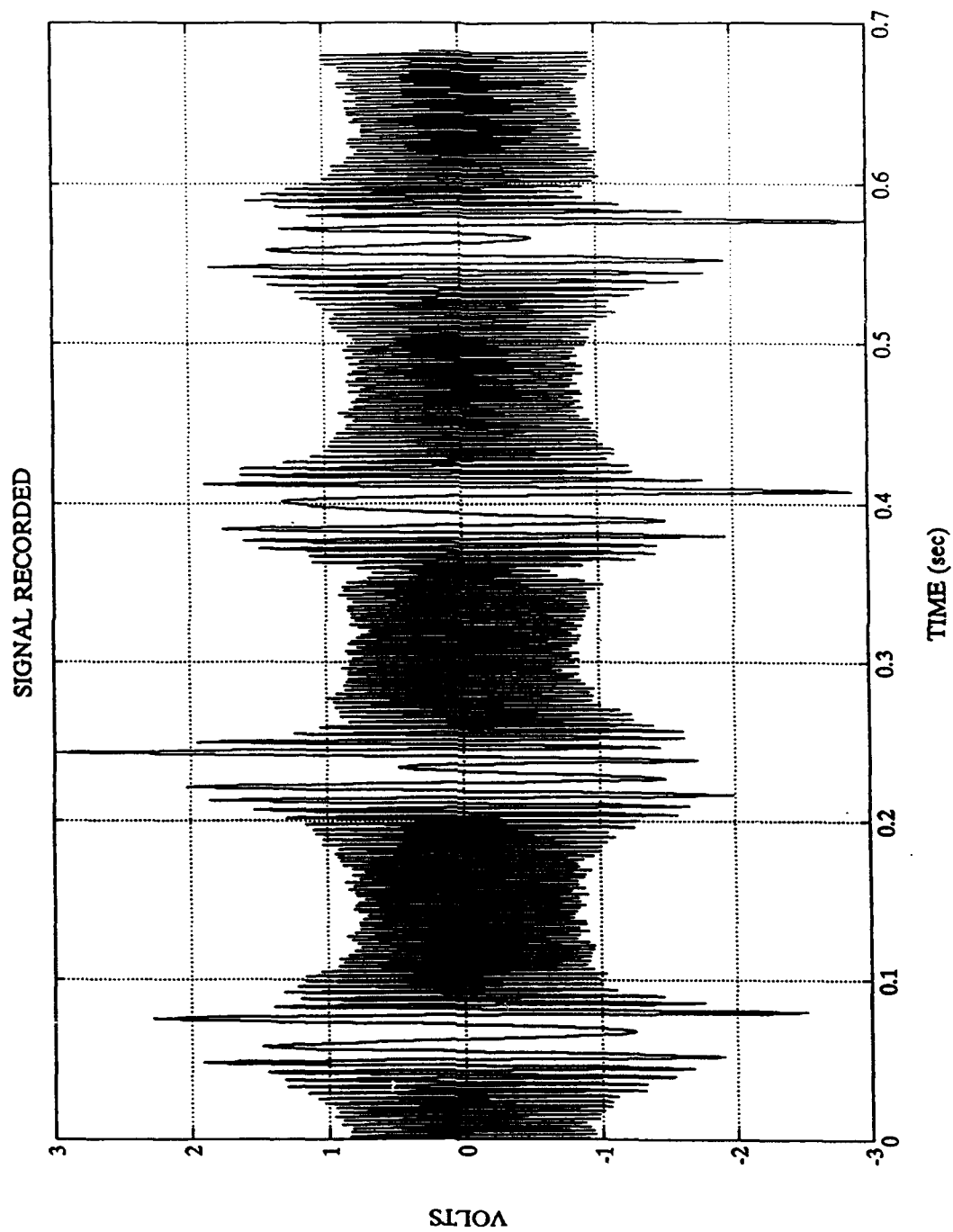


Fig. 8 - Time domain spectrum obtained with the pendulum tightly constrained, the wind tunnel turned off, and no additional aerodynamic structure.

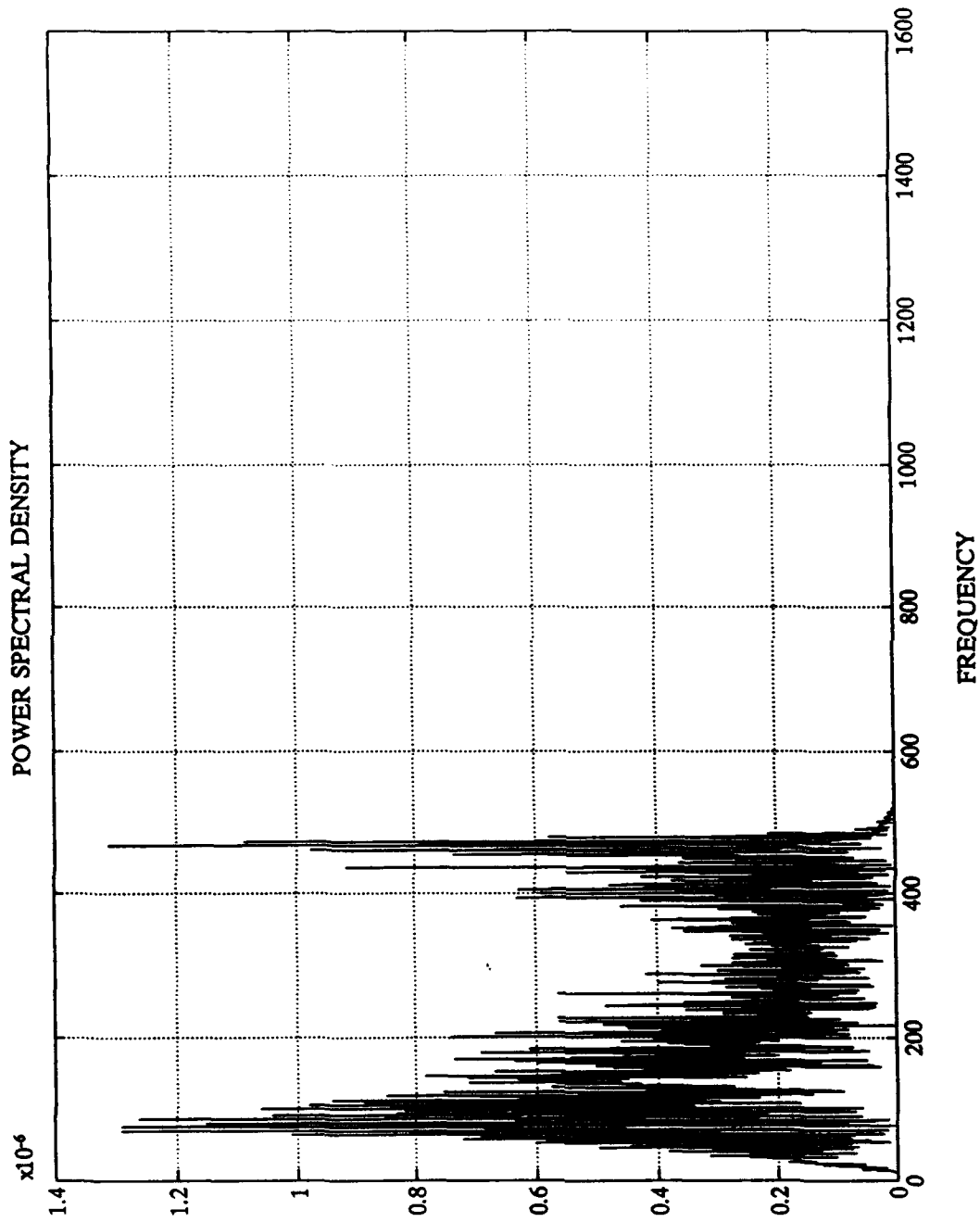


Fig. 9 - Frequency domain spectrum obtained with the pendulum tightly constrained, the wind tunnel turned off, and no additional aerodynamic structure.

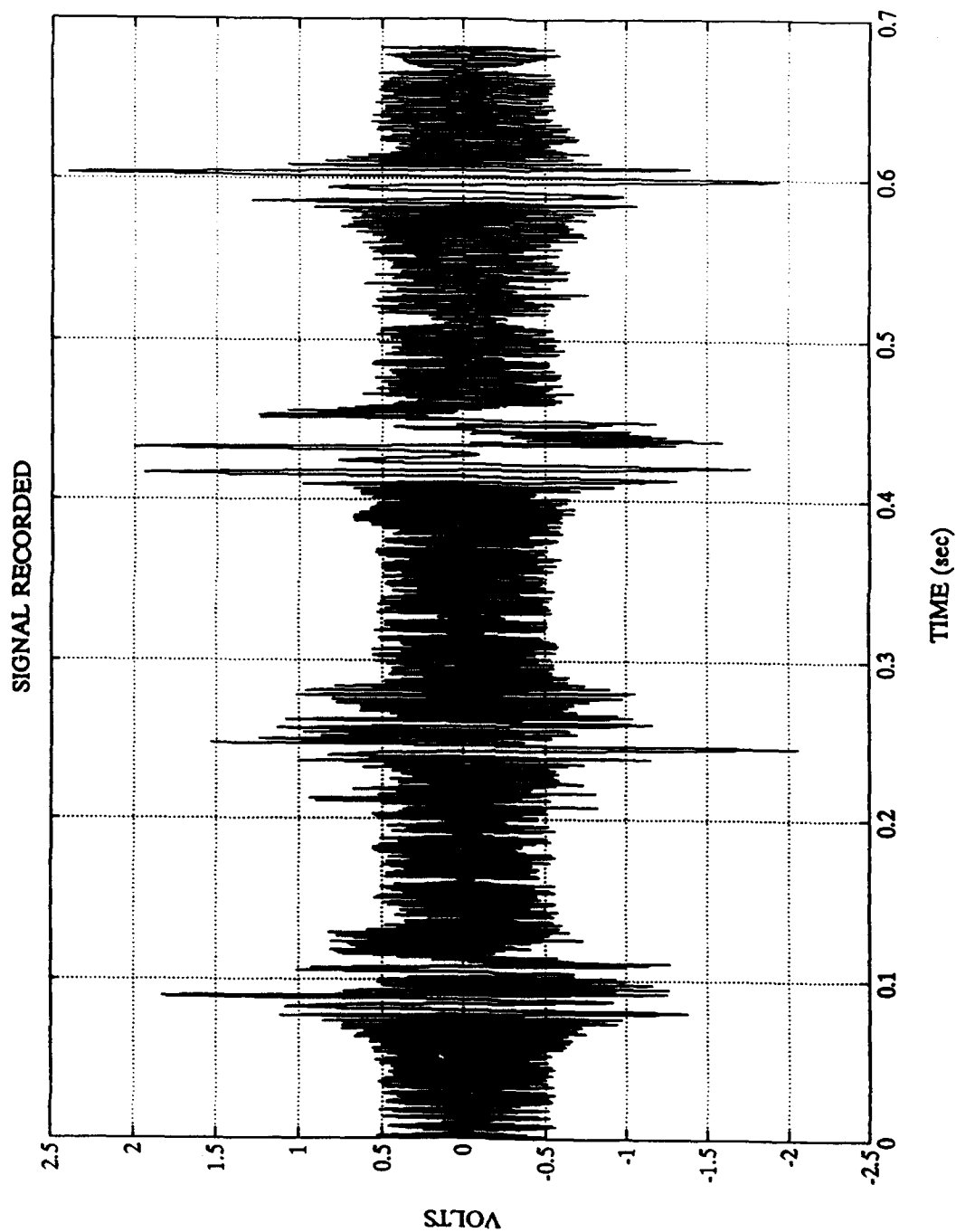


Fig. 10 - Time domain spectrum obtained with the pendulum free to move, the wind tunnel turned off, and no additional aerodynamic structure.

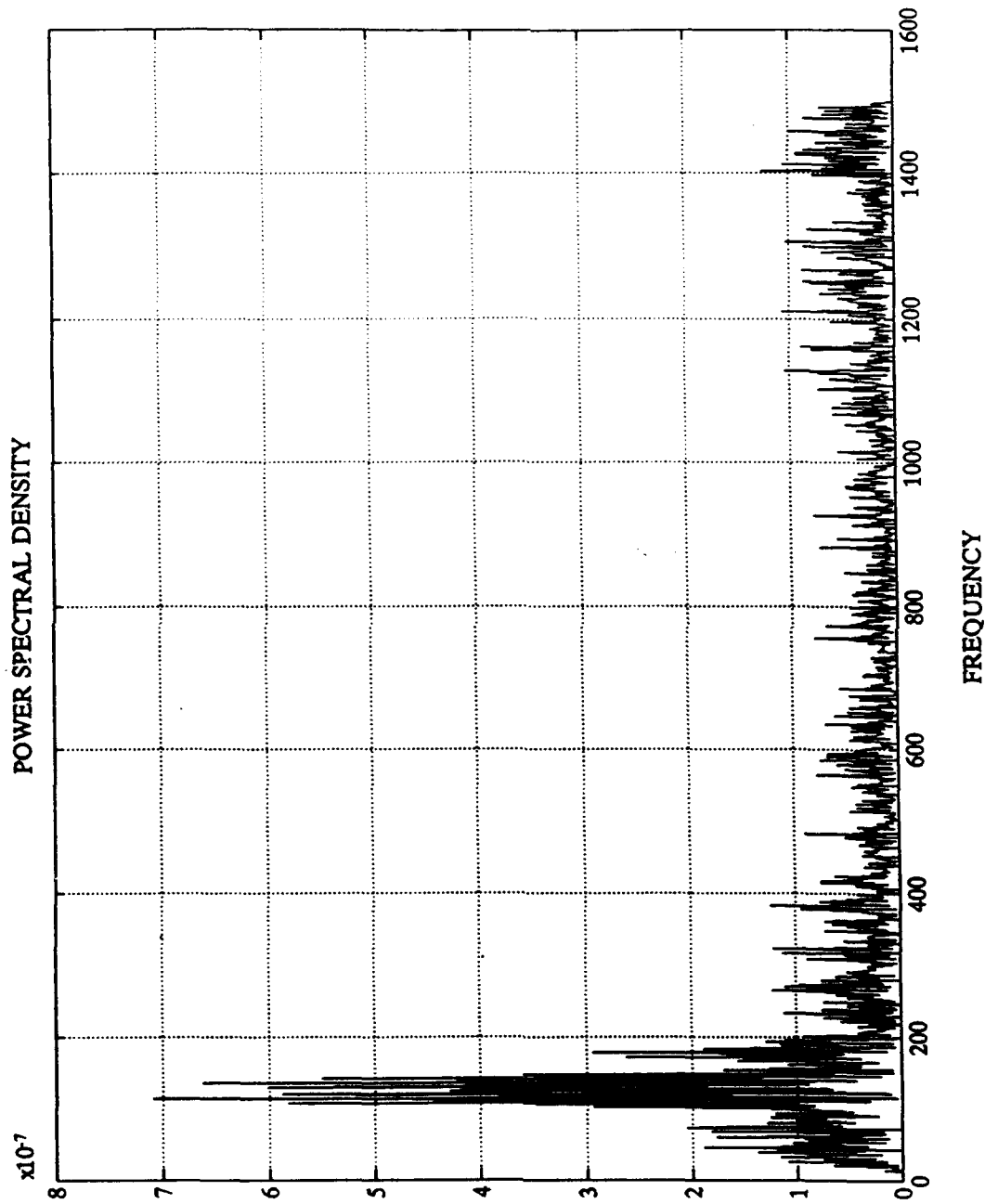


Fig. 11 - Frequency domain spectrum obtained with the pendulum free to move, the wind tunnel turned off, and no additional aerodynamic structure.

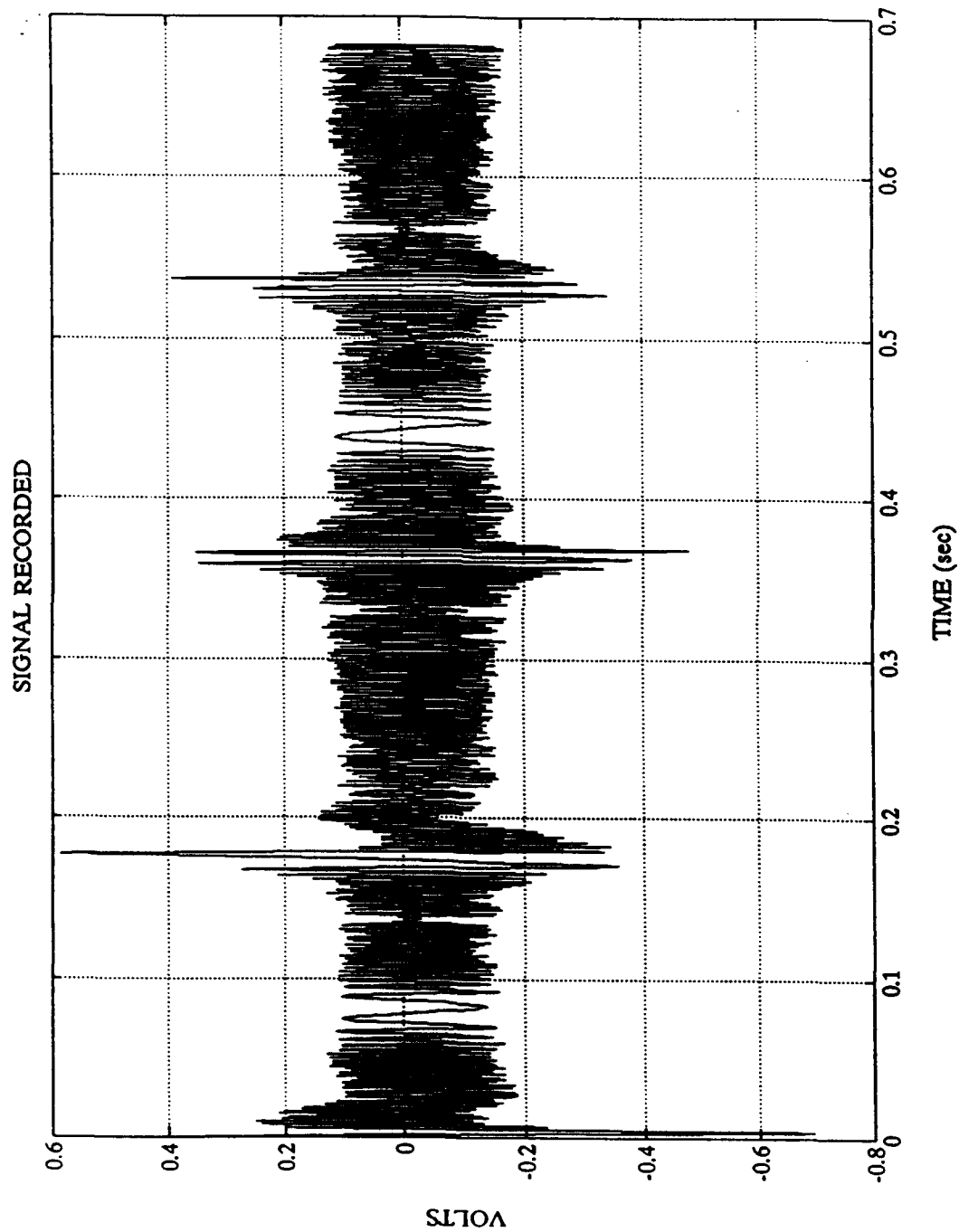


Fig. 12 - Time domain spectrum obtained with the pendulum tightly constrained, the wind tunnel turned off, and an additional aerodynamic structure attached.

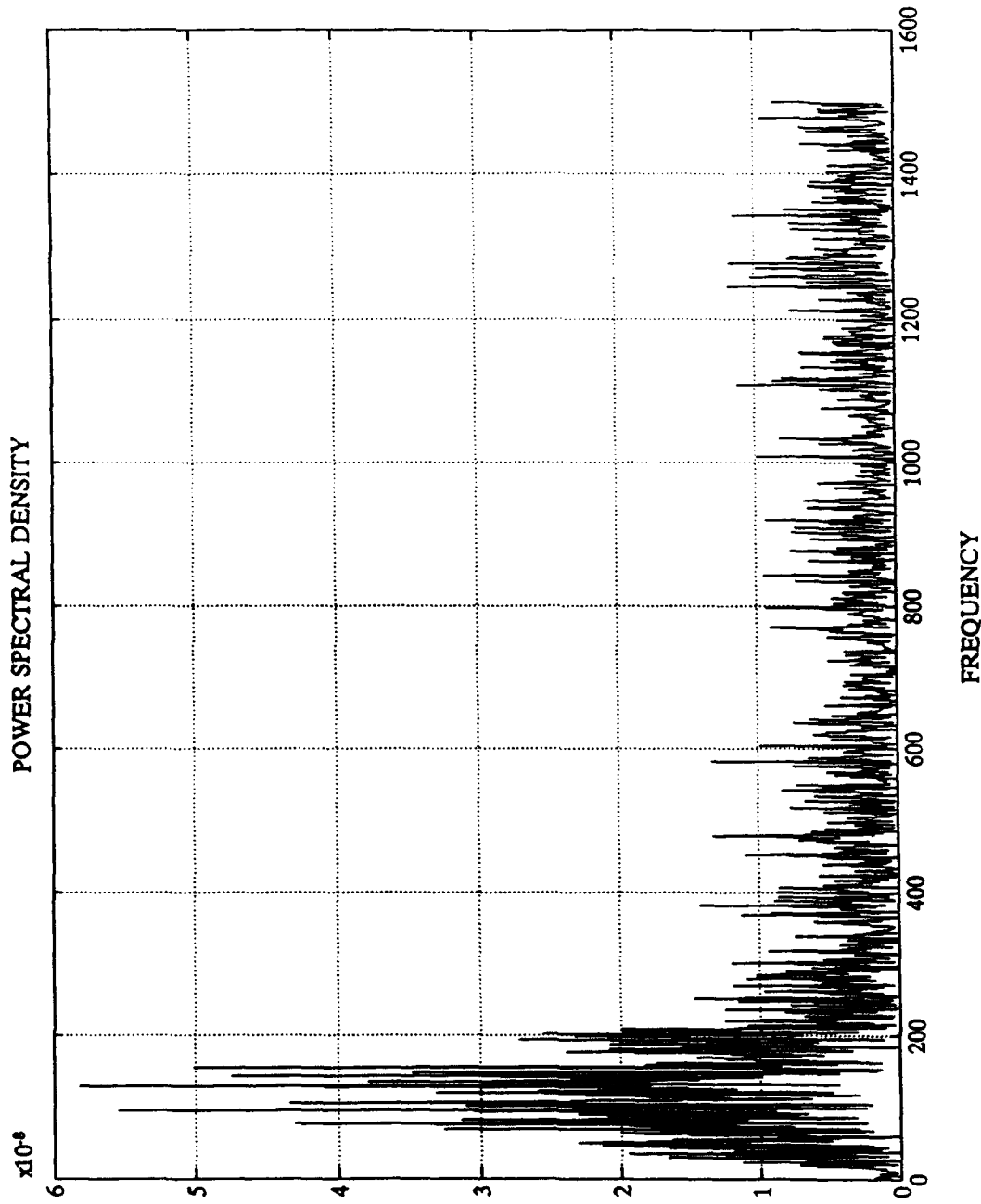


Fig. 13 - Frequency domain spectrum obtained with the pendulum tightly constrained, the wind tunnel turned off, and an additional aerodynamic structure attached.

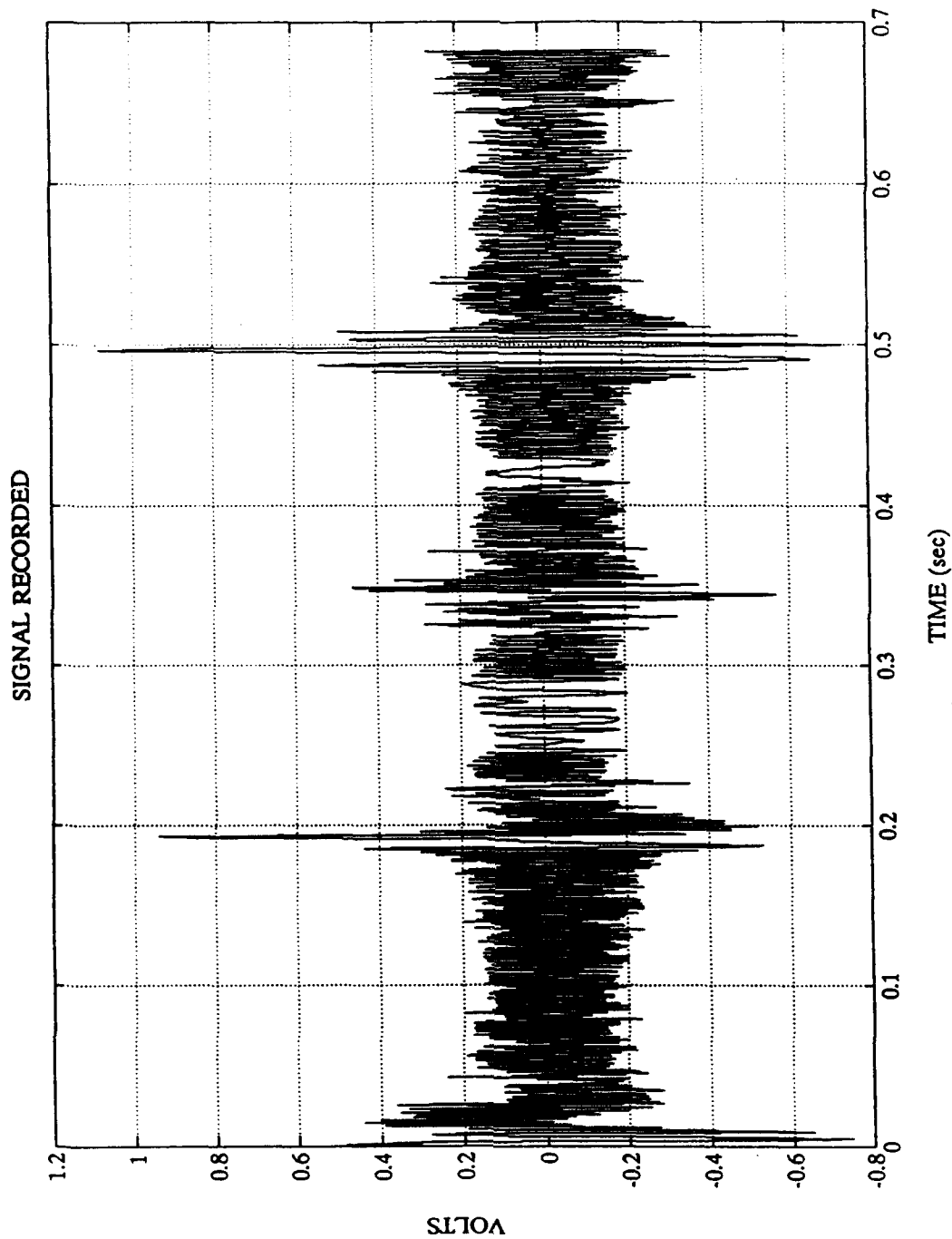


Fig. 14 - Time domain spectrum obtained with the pendulum free to move, the wind tunnel off, and an additional aerodynamic structure attached.

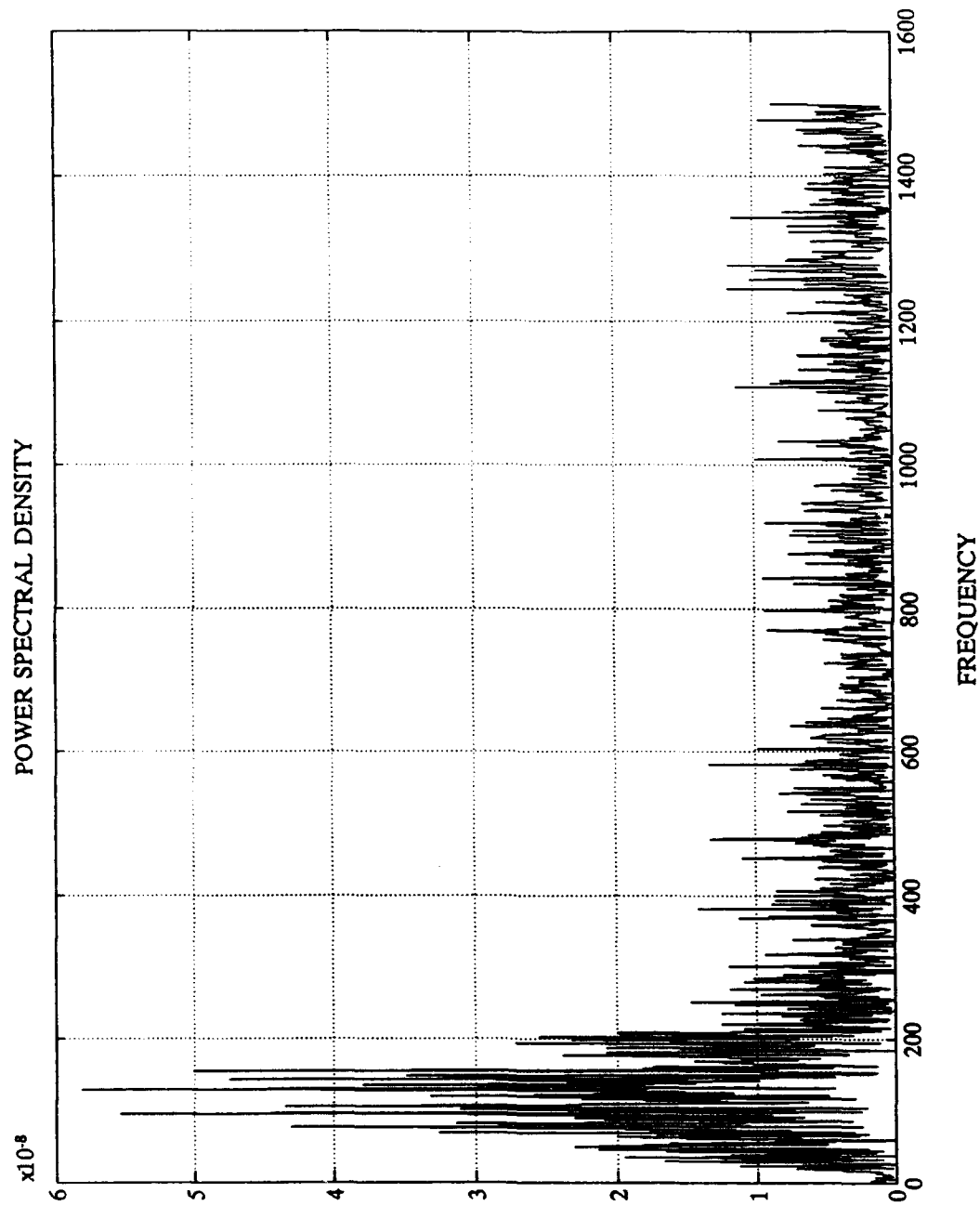


Fig. 15 - Frequency domain spectrum obtained with the pendulum free to move, the wind tunnel turned off, and an additional aerodynamic structure attached.

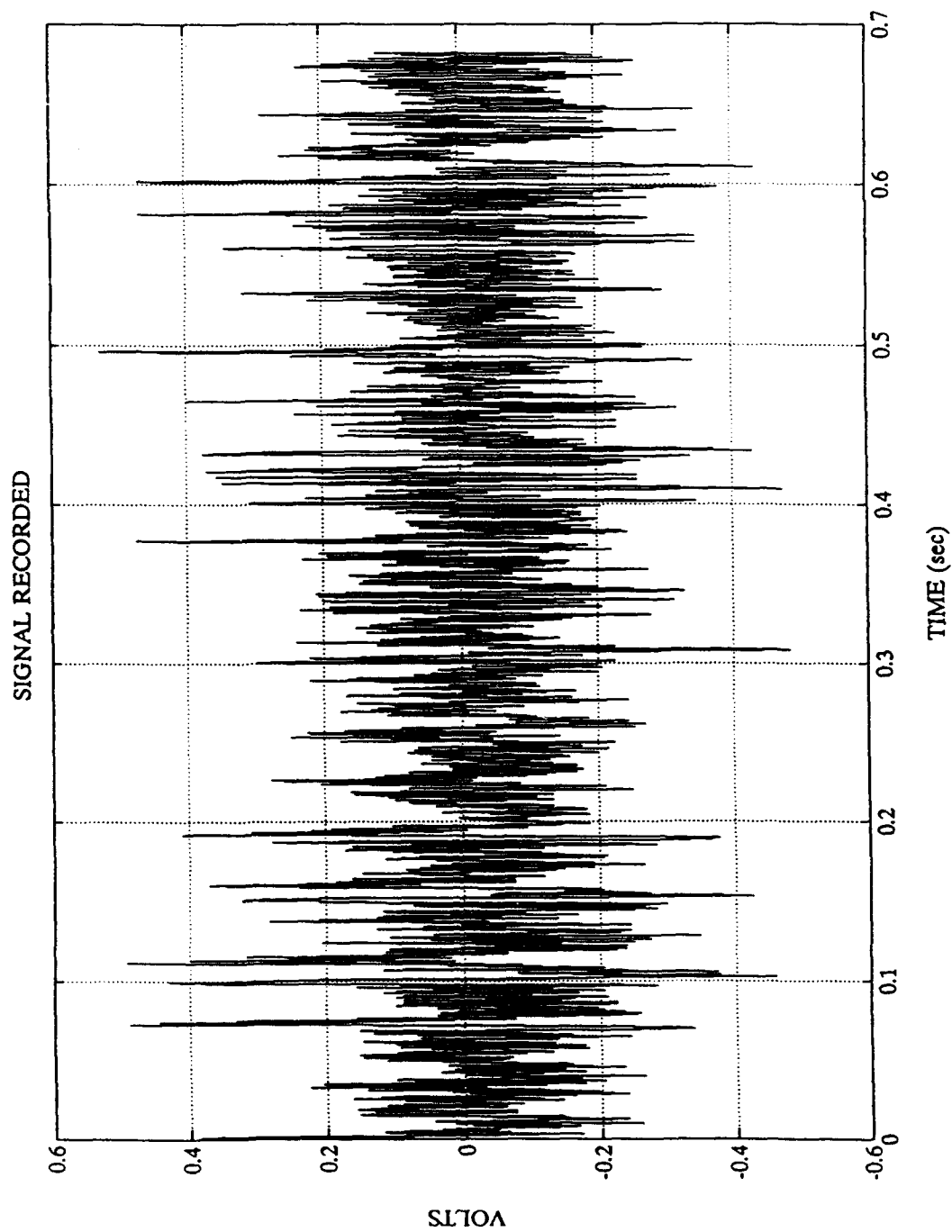


Fig. 16 - Time domain spectrum obtained with the pendulum tightly constrained, the wind tunnel turned on, and no additional aerodynamic structure.

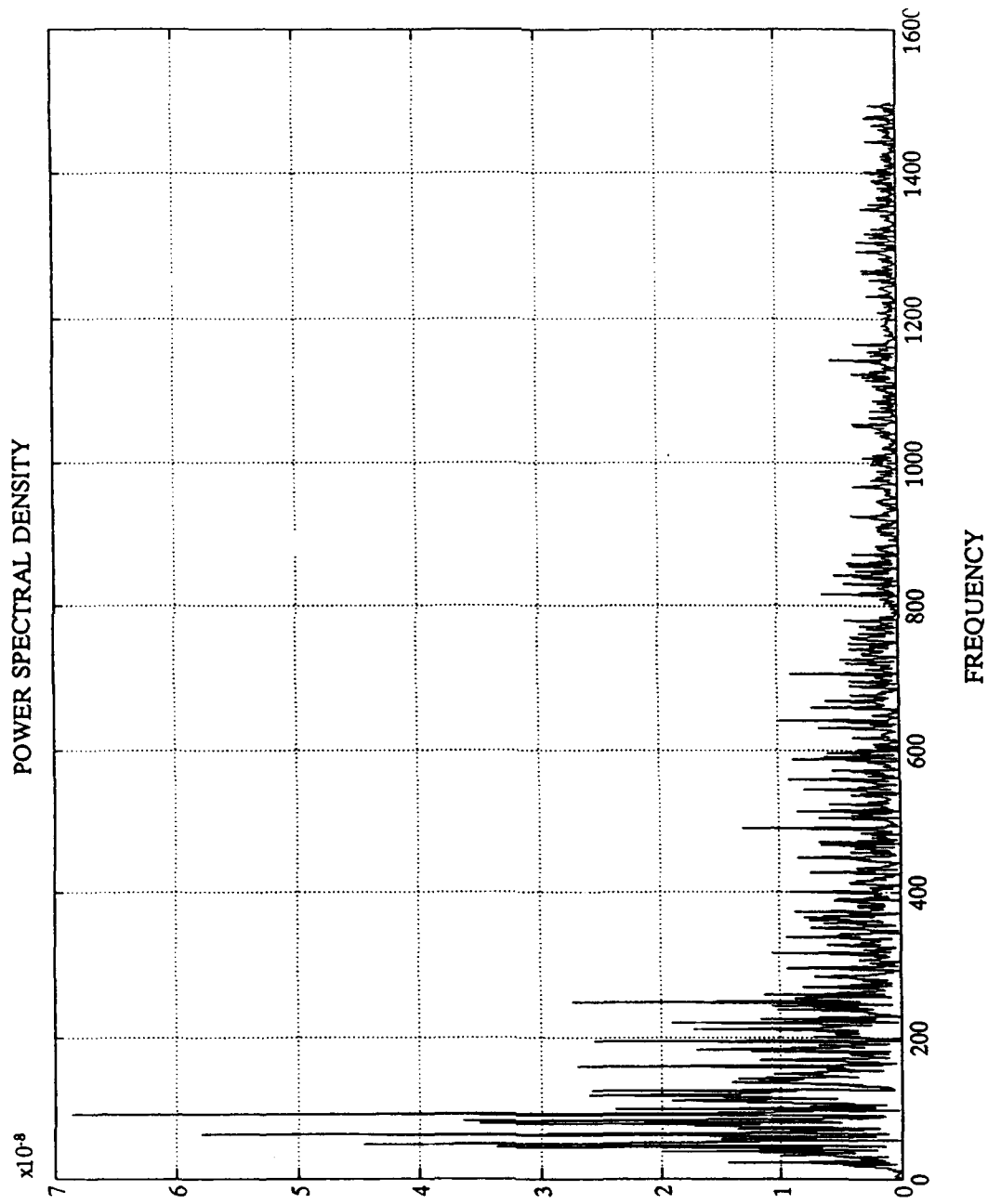


Fig. 17 - Frequency domain spectrum obtained with the pendulum tightly constrained, the wind tunnel turned on, and no additional aerodynamic structure.

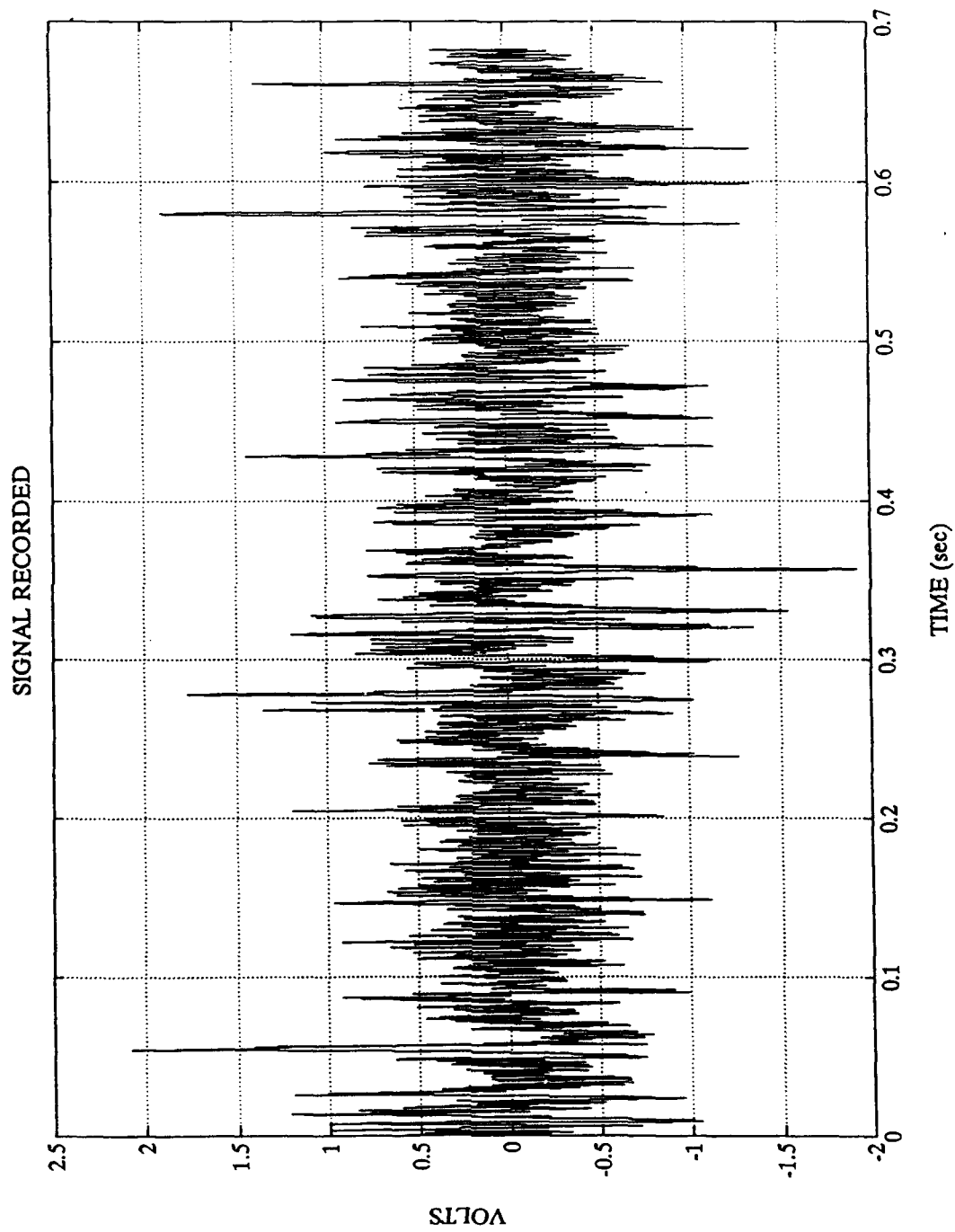


Fig. 18 - Time domain spectrum obtained with the pendulum free to move, the wind tunnel turned on, and no additional aerodynamic structure.

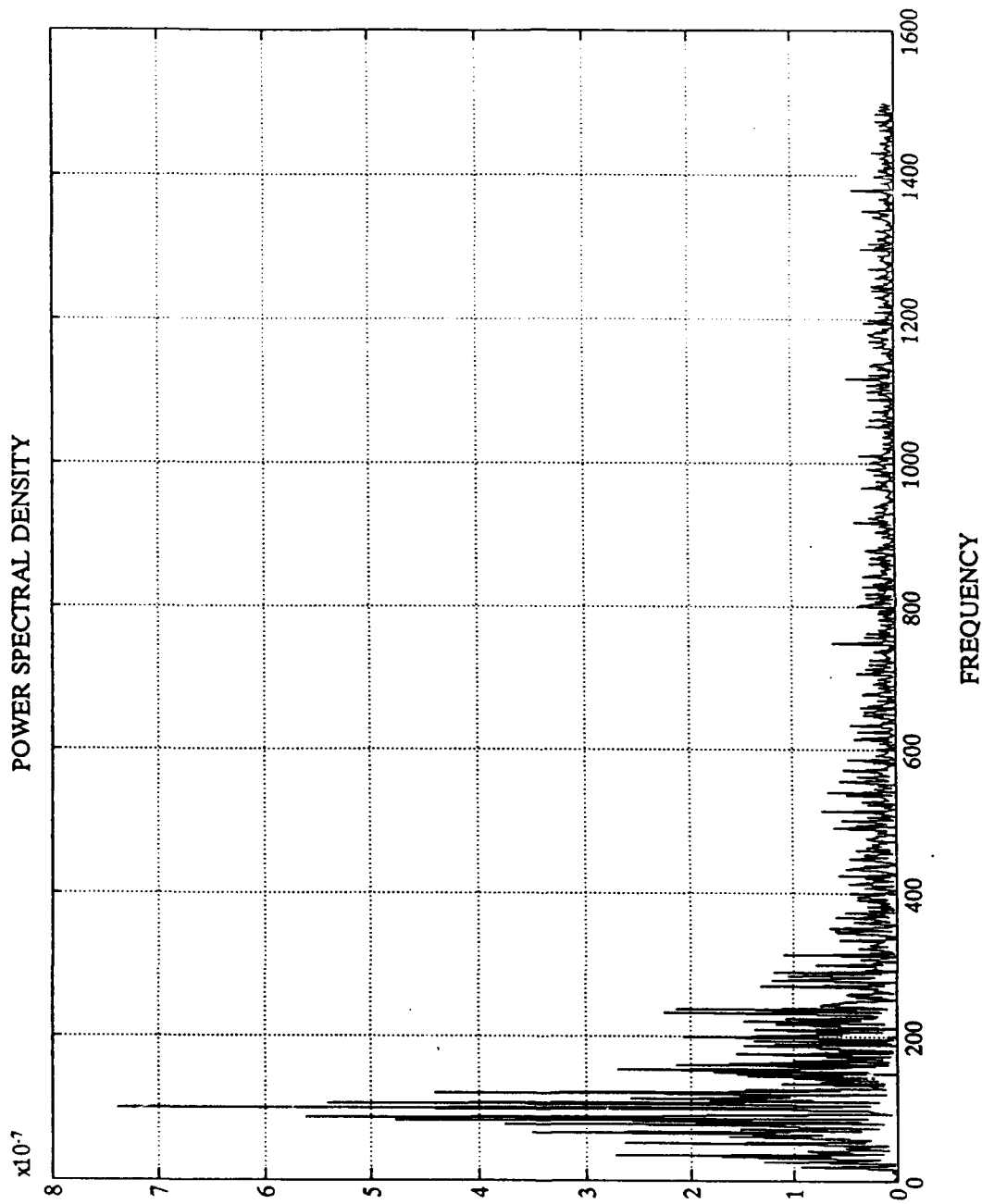


Fig. 19 - Frequency domain spectrum obtained with the pendulum free to move, the wind tunnel turned on, and no additional aerodynamic structure.

### 3. Limitations

The output of this particular optical strain gauge, unlike that of conventional foil gauges is a constant plus the cosine of the integral of strain over the extent of the gauge in the material. This is seen by substituting Eq. 11 into Eq. 1 to obtain Eq. 16.

$$i = E^2 \left( 1 + \cos \left( \frac{12\pi D(t)}{\lambda_0 L} (n-C) (|y_1| + |y_2|) \right) \right) = E^2 (1 + \cos(zD(t))) \quad (16)$$

There is no one to one correspondence between optical gauge output and strain. Because the cosine is an even function, a positive strain gives the same output as a negative strain. This ambiguity, as a practical matter, is a severe limitation in the usefulness of the gauge outside of controlled experimental settings.

If the optical gauge output included a sign on the strain, the gage output peaks could be counted electronically to obtain a one to one correspondence of gauge output with strain. This is in principle possible with a more complex gauge configuration which would include a third optical fiber. However, the accuracy and material stability required for this additional feature seems to be inconsistent with the dimensional stability of composite materials involved.

When an optical fiber is used as part of a smart skin,

multiple roles are usually envisioned for it. One role is the measurement of mechanical strain, but others include the information channel in a fly-by-wire control system, communication channels, and various damage detection systems which depend on optical continuity. In these latter roles, the fibers necessarily extend long distances through the structure. In the strain gauge application, the optical fiber, like any other strain gauge, will yield only an integrated value over the active length of the gauge. Therefore, another important limitation on this type of strain gauge, as part of a multiple use system, is that the strain reading will only be an integrated average over the entire length of the fiber which is embedded within the structure. In some modes of vibrational motion, such as that illustrated in Fig. 20, the gauge reading will average to zero no matter what the strains are at individual points. In any case, the shape into which the structure is strained must be known in order to interpret quantitatively the reading of an optical strain gauge.

The structure chosen to calibrate the gauge is shown in Fig. 2. Although it is not theoretically necessary to run both of the fibers through the structure, it is worthwhile to do so. This system is very sensitive to mechanical noise, and to obtain noise cancellation, both fibers should be in the same environment. The price for this cancellation is that the strain measurement becomes a measurement of the

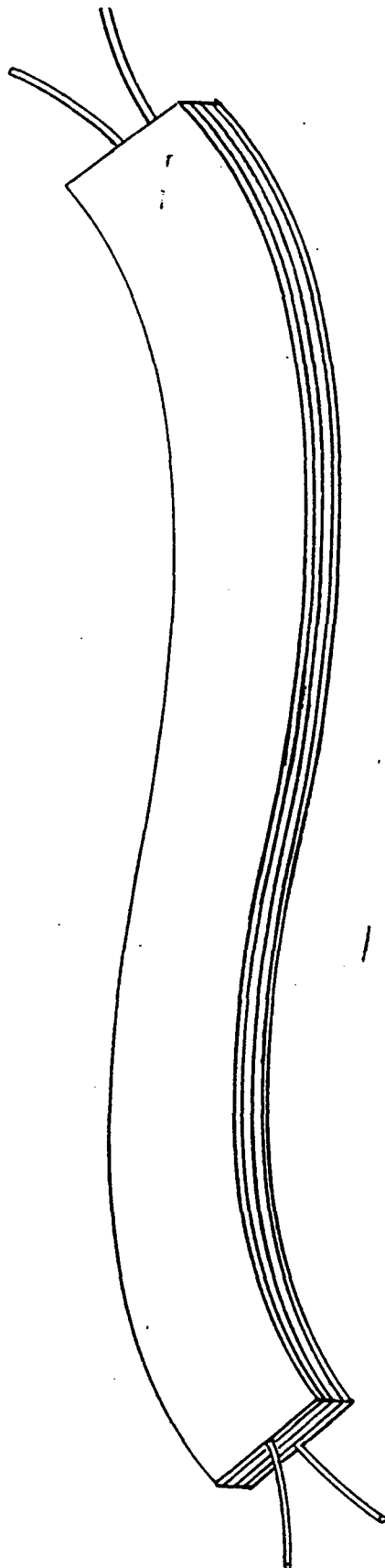


FIG. 20  
Optical Strain Gauge Reading  
Averages to Zero

difference in strains in different portions of the structure. Thus if the specimen in Fig. 2 had been put in tension rather than in bending, the gauge would read zero no matter what the strain.

### CONCLUSIONS

One conclusion drawn from this work is that optical strain gauges of the type studied are about as sensitive to mechanical strain as conventional foil strain gauges. On the other hand, they do not offer an output with a one to one correspondence with strain. Difficult forms of signal processing would often be required to obtain useful quantitative information on strain. In many real life situations, the averaging necessarily present would mask important strain information. However, the output of the optical gauge converts the first time derivative of structural strain into frequency in the audible domain. For the different configurations tested, the corresponding audio signals were easily distinguished, one from another. Therefore it is possible that, for a particular structures driven by particular forces, the output from this optical strain gauge system could be useful in a subjective evaluation of mechanical integrity.

## APPLICATIONS

In one possible application of this type of system optical strain gauges could be placed in critical portions of an aircraft. The signal produced from the optical strain gauges could be recorded during a flight, and the recording analyzed to determine high strain flights, or to identify specific incidents that may have damaged the structure. In addition, if a pilot undergoes a maneuver or situation that he feels has put undue strain on the aircraft, he can tune in to the optical strain gauge signal to monitor the structure in real time.

The potential utility of such a system is not limited to aircraft. It could be used to monitor any structure in which optical fibers are embedded or attached in a manner that the strain of the structure is communicated to the fibers. The basic idea is to study the signal and get a baseline of what the initial "healthy" signal looks and sounds like. Any deviation from this baseline will give an indication that something is wrong.

## FUTURE WORK

In this work, only the mechanical configuration of the specimen was altered. Future work might entail changing the

weight of the pendulum within the box to determine the minimum threshold level at which differences in the signal could be detected. An additional change in the model might include variations the stiffness of the beam. This could be accomplished by testing several composite specimens with different degrees of stiffness. Finally, testing specimens to the point of failure would provide data on actual, as opposed to modeled, damage. These areas reflect investigation of models more representative of structural damage in actual aircraft.

One additional area of future work would be to study more sophisticated methods of analyzing frequency domain data. Better analysis in this area would provide additional information for use in detecting differences in recorded signals.

**BIBLIOGRAPHY**

Butler, C. D. and G. B. Hocker, "Fiber Optics Strain Gauge," Applied Optics, Vol 17(1978), pp. 2667-2669.

Cole, J. H., et al., "Advances in Optical Fiber Sensors," SPIE, Vol 269(1981), pp. 115-124.

Giallorenzi, T., et al., "Optical Fiber Sensors Challenge the Competition," Spectrum, IEEE, (Sept. 1986), pp. 44-49.

Giallorenzi, T., et al., "Optical Fiber Sensor Technology," Quantum Electronics, IEEE, (April 1982), pp. 626-664.

Jackson, D. A., et al., "Elimination of drift in a single-mode optical fiber interferometer using a piezoelectrically stretched coiled fiber," Applied Optics, Vol. 19(1980), pp. 2926-2929.

Jones, W. B., Introduction to Optical Fiber Communication Systems, Holt, Rinehart and Winston, Inc., New York, 1988.

Mazur, C. J., et al., "Air Force Smart Structures/Skins Program Overview," SPIE, Vol. 986(1988), pp. 19-29.

Measures, R. M., et al., "Structurally Integrated Fiber Optic Damage Assessment System For Composite Materials," Applied Optics, Vol. 28(1989), pp. 2626-2633.

Park, E. D., "Fiber Optic Sensing in the Military," Sensors, (Jan. 1986), pp. 14-19.

Robinson, D. A., "Failure Modes in Composite Materials," USNA Trident Scholar Project Report, No. 148(1987).

Stremmler, F. G., Introduction to Communication Systems, Addison-Wesley Publishing Company, Inc., New York, 1990.

Tay, A. And D. Wilson, "Strain Analysis of Optical Fibers Embedded in Composite Materials Using Finite Element Modeling," Fiber Optic Smart Structures and Skins II, SPIE, Vol. 1170, pp. 521-533.

Valis, T., et al., "Localized Fiber Optics Strain Sensors Embedded in Composite Materials," Fiber Optic Smart Structures and Skins II, SPIE, Vol. 1170, pp. 495-504.

Welborn, M. L., "The Behavior of a Composite Material in Compression," USNA Trident Scholar Project Report, No. 163(1989).

## APPENDIX A

### Beam Deflection Calculations

Since the specimen as shown in Fig. 4 is symmetric, just one half of it is reproduced in Fig. A1. The usual equation for an ordinary beam in bending is given by the expression in Eq. A1.

$$EI * \frac{d^2y}{dx^2} = M \quad (A1)$$

Here E is the modulus of the homogeneous and isotropic material, I is the moment of inertia of the beam cross section and M is the moment at any distance, x. In the Fig. A1, this moment is given in Eq. A2.

$$M = \left( \frac{L}{2} - x \right) * F \quad (A2)$$

Here, F is the force pushing up at the support L/2 inches from the beam center. These equations are united in Eq. A3.

$$\frac{d^2y}{dx^2} = \left( \frac{F}{EI} \right) * \left( \frac{L}{2} - x \right) \quad (A3)$$

For composite structures, E and I are complex functions of materials and geometry and are not usefully defined separately. However, the product, (EI), is termed "beam stiffness" and is well defined. It can be measured if the force, F, is also

measured along with D. In this work, F was not measured and so only the ratio F/EI will be obtained. The relation between F/EI and D is given in Eq. A4.

$$\left(\frac{F}{EI}\right) = \frac{3 \cdot D}{\left(\frac{L}{2}\right)^3} = \frac{24 \cdot D}{L^3} \quad (\text{A4})$$

When integrated twice, and  $y=0$  when  $x=0$  as shown in Fig. A1, the expression for the shape of the deflected beam is given in Eq. A5.

$$y = \left(\frac{F}{EI}\right) * \left(\frac{\frac{L}{2}}{2} * x^2 - \frac{1}{2 \cdot 3} * x^3\right) = \frac{24 \cdot D}{L^3} * \left(\frac{L}{4} * x^2 - \frac{1}{6} * x^3\right) \quad (\text{A5})$$

The curvature of the beam is given approximately by the expression in Eq. A6.

$$K = \frac{1}{R} = \frac{d^2 y}{dx^2} = \left(\frac{F}{EI}\right) * \left(\frac{L}{2} - x\right) \quad (\text{A6})$$

Here,  $k$  is the beam curvature and  $R$  is the radius of curvature.

Replacing F/EI in Eq. A6 with the expression in Eq. A5, the curvature as a function of beam deflection, D, and the distance along the beam,  $x$ , is determined.

$$K = \left(\frac{24 \cdot D}{L^3}\right) * \left(\frac{L}{2} - x\right) \quad (\text{A7})$$

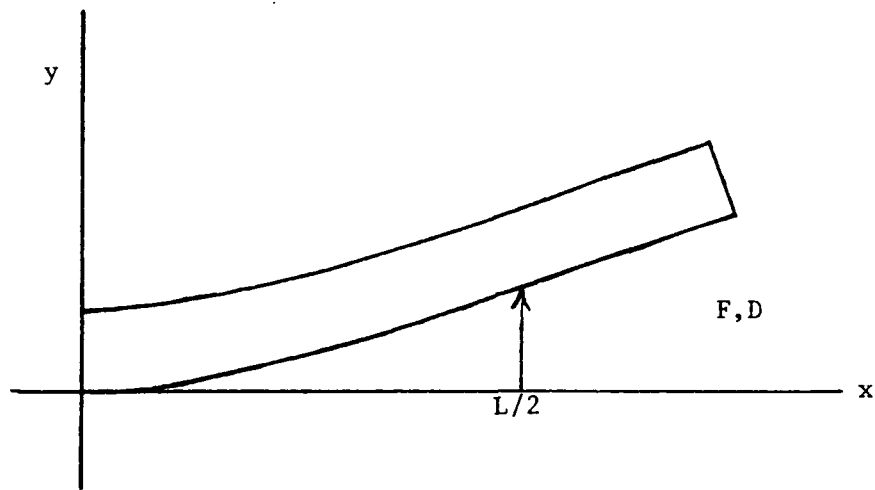


FIG. A1

Beam Deflection Geometry

## APPENDIX B

### Longitudinal Strain Calculation

Using similar triangles in Fig. B1, the relation in Eq. B1 is obtained.

$$\frac{L}{R} = \theta = \frac{\delta L}{v} \quad (\text{B1})$$

Since  $\delta L/L = \text{strain}, e$ , we get Eq. B2.

$$e = \frac{\delta L}{L} = -\frac{v}{R} = -v * K \quad (\text{B2})$$

Here,  $v$  is the distance up from the center or neutral axis of the beam to the point within the beam where the strain is wanted and, as before,  $K = 1/R$  is the beam curvature. From Fig. B1, it can be seen that positive values of  $v$  results correspond to negative or compressive strain.

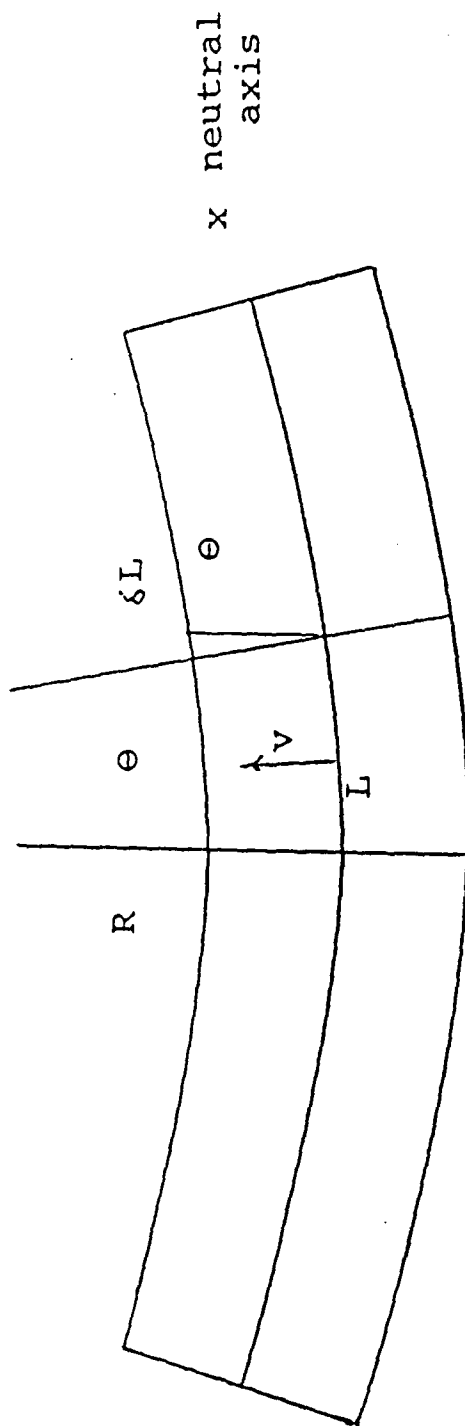


Fig. B1

## APPENDIX C

### Sampling Theory

In order to provide a means of quantitatively analyzing the signals obtained in the second experiment, it was necessary to sample these signals digitally for analysis by a computer. This was done through the use of the DT 2801 analog to digital converter board, which converts analog signals, such as the signal from the photodetector, into a digital format. The program used is listed as Program C1 at the end of this Appendix. This program allowed the user to input the number of samples to be taken as well as the rate at which they were taken. The sampled signal was then written to a file and stored in a PC.

Utilizing MATLAB software, this file was read into a matrix, which could easily be manipulated. The program used in this section is listed as Program C2 at the end of this Appendix. It is a menu driven program which allows the user to acquire new data or analyze previously sampled data. The analysis portion includes plots of the time domain and frequency domain, and allows specified regions of the plots to be enlarged. Samples of these plots are shown in Fig. 8 to Fig. 19.

The frequency domain analysis consisted of evaluating the

power spectral density. Fourier theory states that periodic signals, such as the ones that were sampled in this experiment, are made up of the sum of sine waves oscillating at different frequencies. The signals were sampled at a given period,  $T_s$ , for an interval of time,  $T_u$ . The fundamental frequency,  $f_0$ , of this sampling is then  $1/T_u$ . The Fourier spectrum exists only at discrete values of this fundamental frequency,  $f_0$ . This spectrum is represented graphically by placing points at the discrete frequency values,  $f = 0, \pm f_0, \pm 2f_0, \dots$ , with their heights proportional to the power of the corresponding frequency components. The power spectral density thus shows the distribution of the frequencies of these sine waves.

In order to plot the power spectral density the Fast Fourier Transform (FFT) of the signal must be determined. The Fourier transform of a function  $f(t)$  is shown in Eq. C1.

$$F(\omega) = \mathcal{F}\{f(t)\} = \int_{-\infty}^{+\infty} f(t) e^{-j\omega t} dt \quad (C1)$$

The discrete Fourier transform, DFT, is shown in Eq. C2.

$$F_D(n\Omega) = \sum_{k=0}^{N-1} f(kT) e^{-j\Omega T n k}, n=0, 1, \dots, N-1 \quad (C2)$$

where  $\Omega = 2\pi/(NT)$ . The DFT does not account for the factor  $dt$  in the continuous integral of the Fourier transform. To account for this each element in the matrix,  $x$ , was multiplied by the period,  $T_s$ . The FFT, a more efficient algorithm for

the DFT, is then performed on this new matrix,  $x_1$ . However, the FFT assumes the signal is periodic as in Fig. C1. To account for this periodic assumption, the signal must be convolved with a series of impulse functions which are spaced  $T_u$  seconds apart. In the frequency domain, this translates to a series of impulse functions  $1/T_u$  Hz apart. This relation is shown in Fig. C2. To achieve this process in the computer program the FFT of the matrix  $x_1$  was obtained and then multiplied by the fundamental frequency,  $f_0$ . Finally this matrix,  $x_2$ , was multiplied by its complex conjugate to produce a real number for plotting. The final matrix,  $xpsd$ , contained the power spectral density components and was plotted versus frequency. A typical power spectral density plot is shown in Fig. 9.

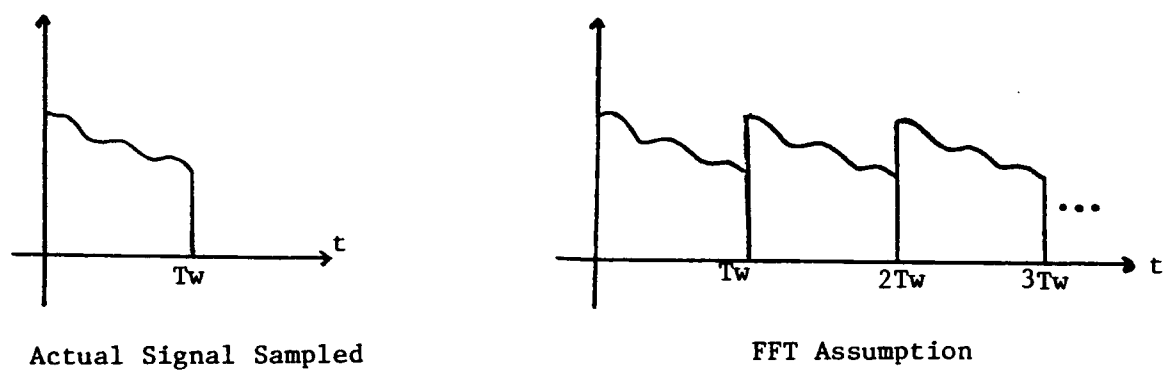


FIG. C1

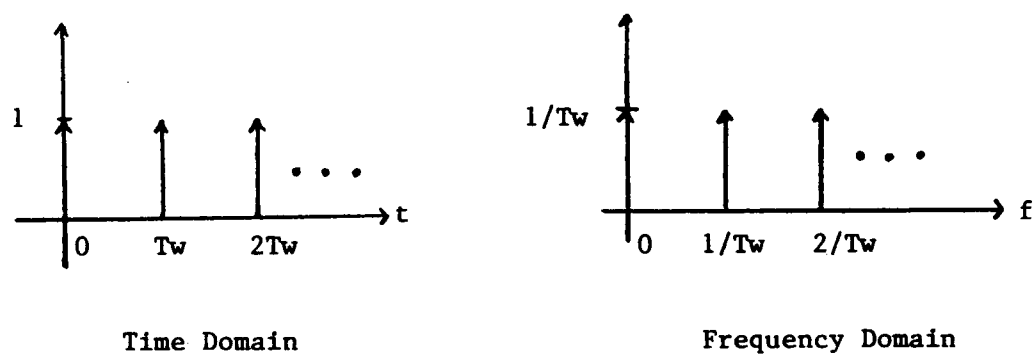


FIG. C2

Program C1 - Basic program to acquire data from external analog signal, convert to digital signal, and store data points in a file.

```
' read vector of values from adc 1
' external trigger, active low.
' Quick Basic 4.5

REM $INCLUDE: 'pcldefs.bi'
CLS
COLOR 6
LOCATE 1,1
PRINT "                                PC LAB DATA ACQUISITION"
PRINT
INPUT "ENTER THE DATA FILE NAME (EXAMPLE: x1file): ",FILENAME$
PRINT
IF FILENAME$="" THEN FILENAME$="signal"
INPUT "ENTER NUMBER OF SAMPLES : ", N%
IF N%=0 THEN N%=2048
PRINT
DIM AA%(N%)
ER% = 0
status% = SET.ERROR.CONTROL.WORD(ER%)
HIGH.V! = 10!
LOW.V! = -10!
RANGE! = HIGH.V! - LOW.V!
NOC! = 4096!
LSB! = RANGE! / NOC!'VOLTS PER BIT
TIMING.SOURCE% = 2 'EXTERNAL TRIGGER, INTERNAL CLOCK
CHAN% = 1
GAIN% = 1
status% = SETUP.ADC(TIMING.SOURCE%, CHAN%, CHAN%, GAIN%)
status% = GET.ERROR.CODE(ER%)
INPUT "ENTER THE PERIOD : ", PERIOD
IF PERIOD=0 THEN PERIOD=.00033333
status% = SET.CLOCK.PERIOD(PERIOD)
status% = DISABLE.SYSTEM.CLOCK
LOCATE 20,20
PRINT "**** WAITING FOR EXTERNAL TRIGGER ****"
status% = ADC.SERIES(N%, AA%(0))
IF status% <> 0 THEN PRINT "Status after adc.series "; status%
status% = ENABLE.SYSTEM.CLOCK
status% = GET.ERROR.CODE(ER%)
OPEN "O", #1, FILENAME$ + ".m"
PRINT #1, "x=["
FOR I% = 0 TO N% - 2
    PRINT #1, LOW.V! + AA%(I%) * LSB!
NEXT I%
PRINT #1, LOW.V! + AA%(N% - 1) * LSB!; "]"
PRINT #1, "period="; PERIOD; ";"
PRINT #1, "time="; TTOTAL; ";"
CLOSE #1
END
```

Program C2 - MATLAB .m file to read data in from file, and determine and manipulate the frequency and time domain spectrum.

```
% display signal read from A/D converter
% find and display power spect density
clear;
clc;
contin=1;
newdata=1;
while (contin==1)
    flag1=1;
    flag2=1;
    flag3=1;
    while (flag1==1)
        clc
        disp('WOULD YOU LIKE TO ACQUIRE DATA ? ');
        disp('');
        disp('      (1) YES ');
        disp('      (2) NO  ');
        disp('');
        resp=input('SELECTION : ');
        disp('')

        if (resp==1)
            !dt
            clc
            end;

        if (resp==2)
            flag1=0;
            end;

    end; % while flag1=1

    clc;
    if newdata==1
        disp('');
        disp('');
        disp('');
        disp('');
        DATA ANALYSIS
        ');
        t=input('PLEASE ENTER THE DATA FILE NAME (EXAMPLE: x1file ):');
    end;
    clc;
    oldx=x;
    s=length(x);
    timel=period*[0:s-1];
    plot(timel,x);grid;
    title('SIGNAL RECORDED');
    xlabel('TIME (sec)');
    ylabel('VOLTS');
    pause;

    limits=axis;axis;
    lowy=limits(3);
    highy=limits(4);
    while (flag2==1)
        clc
        disp('*** TIME DOMAIN MENU *** ');
        disp('');
        disp('      (1) CLOSE-UP OF A CERTAIN RANGE ');
        disp('      (2) PRINT CURRENT PLOT  ');
        disp('      (3) CALCULATE FFT OF CURRENT PLOT ');
```

```

disp('      (4) CALCULATE FFT OF ORIGINAL SIGNAL ');
disp('      (5) EXIT THE PROGRAM ');
disp('');
resp=input('SELECTION : ');
disp('')

if (resp==1)
    disp('INPUT RANGES OF TIME FOR CLOSE-UP');
    disp('');
    lowx=input('LOWER TIME : ');
    highx=input('UPPER TIME : ');
    axis([lowx highx lowy highy]);
    plot(timel,x);grid;
    title('SIGNAL RECORDED');
    xlabel('TIME (sec)');
    ylabel('VOLTS');
    axis([1 2 3 4]);axis;
    pause;
    clc;
end;

if (resp==2)
    print;
end;

if (resp==3)
    k=find(timel<lowx);
    lowindex=length(k);
    k=find(timel<highx);
    hiindex=length(k);
    gap=hiindex-lowindex;
    if (gap < 64)
        space = 64;
    elseif (gap < 128)
        space = 128;
    elseif (gap < 256)
        space = 256;
    elseif (gap < 512)
        space = 512;
    elseif (gap < 1024)
        space = 1024;
    else space = 2048;
    end;
    if ((lowindex+space) > 2048)
        hiindex=2048;
        lowindex=hiindex-space;
    else
        hiindex=lowindex+space;
    end;
    x=x(lowindex:hiindex);
    flag2=0;
end;

if (resp==4)
    flag2=0;
end;

if (resp==5)
    flag2=0;
    flag3=0;
end;

```

```

        contin=0;
    end;
    newdata=1;
    end; % while flag2=1

    if flag3==1
        tw=period*s;
        fo=1/tw;
        x1=period*x;
        x2=fft(x1)*fo;
        clear x1;
        f=(0:(s-1))/tw;
        xpsd=x2.*conj(x2)/s;
        clear x2;
        plot(f(2:s/2),xpsd(2:s/2));grid;
        title('POWER SPECTRAL DENSITY');
        xlabel('FREQUENCY');
        pause;

        limits=axis;axis;
        lowy=limits(3);
        highy=limits(4);
    end;

    while (flag3==1)
        clc
        disp('*** FREQUENCY DOMAIN MENU *** ');
        disp('');
        disp('      (1) CLOSE-UP OF A CERTAIN RANGE ');
        disp('      (2) PRINT CURRENT PLOT ');
        disp('      (3) RETURN TO TIME DOMAIN (SAME DATA) ');
        disp('      (4) CONTINUE WITH PROGRAM (NEW DATA) ');
        disp('      (5) EXIT PROGRAM ');
        disp('');
        resp=input('SELECTION : ');
        disp('')

        if (resp==1)
            disp('INPUT RANGES OF FREQUENCY FOR CLOSE-UP');
            disp('');
            lowx=input('LOWER FREQUENCY : ');
            highx=input('UPPER FREQUENCY : ');
            axis([lowx highx lowy highy]);
            plot(f(2:s),xpsd(2:s));grid;
            title('POWER SPECTRAL DENSITY');
            xlabel('FREQUENCY');
            axis([1 2 3 4]);axis;
            pause;
            clc;
        end;

        if (resp==2)
            print;
        end;

        if (resp==3)
            newdata=0;
            flag3=0;
        end;
    end;

```

```
        if (resp==4)
            flag3=0;
        end;

        if (resp==5)
            flag3=0;
            contin=0;
        end;
    end;    % while flag3=1 loop
x=oldx;
end;    % while contin==1 loop
end;
```